



저작자표시-비영리-변경금지 2.0 대한민국

이용자는 아래의 조건을 따르는 경우에 한하여 자유롭게

- 이 저작물을 복제, 배포, 전송, 전시, 공연 및 방송할 수 있습니다.

다음과 같은 조건을 따라야 합니다:



저작자표시. 귀하는 원저작자를 표시하여야 합니다.



비영리. 귀하는 이 저작물을 영리 목적으로 이용할 수 없습니다.



변경금지. 귀하는 이 저작물을 개작, 변형 또는 가공할 수 없습니다.

- 귀하는, 이 저작물의 재이용이나 배포의 경우, 이 저작물에 적용된 이용허락조건을 명확하게 나타내어야 합니다.
- 저작권자로부터 별도의 허가를 받으면 이러한 조건들은 적용되지 않습니다.

저작권법에 따른 이용자의 권리는 위의 내용에 의하여 영향을 받지 않습니다.

이것은 [이용허락규약\(Legal Code\)](#)을 이해하기 쉽게 요약한 것입니다.

[Disclaimer](#)

보건학석사 학위논문

**Degradation kinetics and mechanisms of
hexafluoropropylene oxide dimer acid
(GenX) during VUV photolysis and
VUV/sulfite processes**

VUV 광분해와 VUV/아황산염 공정에서의
hexafluoropropylene oxide dimer acid(GenX) 제거 동역학 및
메커니즘

2023 년 2 월

서울대학교 보건대학원
환경보건학과 환경보건학전공

김 재 희

Degradation kinetics and mechanisms of hexafluoropropylene oxide dimer acid (GenX) during VUV photolysis and VUV/sulfite processes

지도교수 조 경 덕

이 논문을 보건학석사 학위논문으로 제출함
2022 년 11 월

서울대학교 보건대학원
환경보건학과 환경보건학전공
김 재 희

김재희의 석사 학위논문을 인준함
2022 년 12 월

위 원 장 _____ 김 성 균 (인)

부위원장 _____ 이 승 목 (인)

위 원 _____ 조 경 덕 (인)

Abstract

Hexafluoropropylene oxide dimer acid (HFPO-DA), referred to as GenX, has been recently detected in various water bodies, and become a subject of concern due to its environmental persistence and toxicity. In this study, we investigated the degradation of GenX in water under N₂-saturated conditions during vacuum ultraviolet (VUV) photolysis and VUV/sulfite reactions. The decomposition reaction of GenX in all reactions followed the pseudo-first order kinetics. While the removal rate was highest at pH 6 during the VUV photolysis, the removal efficiency increased at high pH conditions in the VUV/sulfite reaction. The hydroxyl radicals (\bullet OH) did not contribute to the degradation of GenX and showed a negative effect during the VUV/sulfite reaction. The transformation products (TPs) of GenX in both reactions were identified using LC-MS/MS and LC-QTOF/MS. Three TPs (TFA, PFPrA, and TP120) were identified in the VUV photolysis reaction while six TPs (TFA, PFPrA (TP164), TP120, TP182, TP186, and TP366) were identified in the VUV/sulfite reaction. Defluorination of GenX was also observed, achieving 17% and 67% for 6 hr in both reactions, respectively. We proposed the degradation pathways of GenX based on the identified TPs and theoretical calculations confirming the reactivity to nucleophilic attack. The initiation reactions for GenX decomposition were found to be C-C bond cleavage, C-O bond cleavage, and sulfonation after decarboxylation. In addition, ecotoxicity prediction using ECOSAR simulation showed that the toxicity of TPs should not be overlooked.

Keyword : GenX; vacuum ultraviolet; hydrated electron; hydrogen atom;
transformation products; defluorination

Student Number : 2021-23110

Contents

List of Tables	iv
List of Figures	v
1. Introduction	1
1.1. Background.....	1
1.2. Previous studies on the degradation of GenX.....	4
1.3. Vacuum ultraviolet (VUV) studies on the degradation of micropollutants.....	7
1.4. Objectives.....	8
2. Materials and Methods	9
2.1. Chemicals.....	9
2.2. Experimental methods.....	10
2.3. Analytical methods.....	12
2.4. Computational methods.....	13
2.5. <i>In silico</i> toxicity assessment.....	14
3. Results and Discussion	15
3.1. Degradation kinetics of GenX.....	15
3.2. Effect of pH.....	19
3.3. Roles of reactive species.....	23
3.4. Identified TPs and defluorination.....	27
3.5. Theoretical calculation and degradation mechanisms.....	32
3.6. <i>In silico</i> toxicity assessment.....	40
4. Conclusions	44
5. References	46
6. Supporting Information	54
국문초록.....	66

List of Tables

Table 1. Physical and chemical properties of GenX (USEPA, 2021).	2
Table 2. Detection cases of GenX in different water matrices in various countries. 3	
Table 3. Previous studies on the degradation of GenX during photochemical AOP and ARP.....	6
Table 4. Calculated Hirshfeld charge and condensed Fukui index f^+ of each atom in GenX.	35
Table 5. The LUMO composition of GenX.....	36
Table 6. Mayer bond order value of GenX ²⁻	37
Table 7. Predicted toxicity for GenX and its TPs using ECOSAR simulation.	42
Table 8. Predicted toxicity for GenX and its TPs using T.E.S.T simulation.....	43

List of Figures

- Fig. 1.** Schematic diagram of the VUV reactor system..... 11
- Fig. 2.** Degradation of GenX during control tests for VUV/sulfite process under anoxic alkaline condition ($[\text{GenX}]_0 = 0.30 \mu\text{M}$, $[\text{sulfite}]_0 = 4.8 \text{ mM}$, $\text{pH} = 10$, $\text{VUV intensity}_{254 \text{ nm}} = 0.65 \text{ mW/cm}^2$, continuous N_2 purging; $n \geq 2$)..... 17
- Fig. 3.** Positive linear correlation with different slopes for pseudo-rate constants of GenX degradation as a function of sulfite concentration during VUV/sulfite process ($[\text{GenX}]_0 = 0.30 \mu\text{M}$, $\text{pH} = 10$, $\text{VUV intensity}_{254 \text{ nm}} = 0.65 \text{ mW/cm}^2$, continuous N_2 purging, $n \geq 2$). 18
- Fig. 4.** Degradation kinetics of GenX at different pH during VUV photolysis and VUV/sulfite ($[\text{sulfite}]_0 = 4.8 \text{ mM}$) processes ($[\text{GenX}]_0 = 3.0 \mu\text{M}$, $\text{VUV intensity}_{254 \text{ nm}} = 0.65 \text{ mW/cm}^2$, continuous N_2 purging, $n = 2$).....21
- Fig. 5.** The change of pH after degradation for 6 h in VUV photolysis ($\text{pH}_0 = 6$) and VUV/sulfite ($\text{pH}_0 = 10$) processes without using buffer solution.....22
- Fig. 6.** Pseudo-first rate constants of GenX degradation in the absence or presence of different radical scavengers during VUV photolysis ($[\text{t-BuOH}] = [\text{NO}_2^-] = [\text{NO}_3^-] = 1 \text{ mM}$, $\text{pH} = 6$) and VUV/sulfite ($[\text{sulfite}]_0 = 4.8 \text{ mM}$, $[\text{t-BuOH}] = [\text{NO}_2^-] = [\text{NO}_3^-] = 6 \text{ mM}$, $\text{pH} = 10$) processes ($[\text{GenX}]_0 = 0.30 \mu\text{M}$, $\text{VUV intensity}_{254 \text{ nm}} = 0.65 \text{ mW/cm}^2$, continuous N_2 purging, $n \geq 2$).....26
- Fig. 7.** Time profiles for the response of identified TPs using (a) LC-MS/MS, (b) LC-QTOF/MS during VUV photolysis ($\text{pH} = 6$), and (c) LC-MS/MS, (d) LC-QTOF/MS during VUV/sulfite ($[\text{sulfite}]_0 = 8.0 \text{ mM}$, $\text{pH} = 10$) processes ($[\text{GenX}]_0 = 3.0 \mu\text{M}$, $\text{VUV intensity}_{254 \text{ nm}} = 0.65 \text{ mW/cm}^2$, continuous N_2 purging; $n = 2$).....30

Fig. 8. Mass balance of fluorine during (a) VUV photolysis (pH = 6) and (b) VUV/sulfite ($[\text{sulfite}]_0 = 8.0 \text{ mM}$, pH = 10) processes ($[\text{GenX}]_0 = 3.0 \text{ }\mu\text{M}$, VUV intensity_{254 nm} = 0.65 mW/cm², continuous N₂ purging; n = 2).31

Fig. 9. (a) Δf isosurface (isosurface value = 0.004) (blue and red surfaces correspond to positive and negative regions, respectively) and (b) LUMO (isosurface value = 0.02) and of GenX at 6-311+g(d,p) level.38

Fig. 10. Proposed degradation pathway of GenX in VUV photolysis and VUV/sulfite processes (blue and red texts correspond to the main TPs of VUV photolysis and VUV/sulfite processes, respectively).39

1. Introduction

1.1. Background

Although per- and polyfluoroalkyl substances (PFASs) have been used in the production of various industrial and consumer products worldwide since the 1940s, they have the characteristics of recalcitrance, bioaccumulation, and long half-lives in the human body (Glüge et al., 2020; Lindstrom et al., 2011). For these reasons, perfluorooctanoic acid (PFOA), a well-known compound among the family of PFASs, has been banned under the international Stockholm Convention in 2019 (UNEP, 2019). In order to deal with the regulation, PFAS alternatives have been recently developed in which a part of the carbon chain is converted into an ether group, or C-F bonds are converted into C-H bonds or C-Cl bonds (Wang et al., 2019b).

Hexafluoropropylene oxide dimer acid (HFPO-DA, Cas No. 13252-13-6) (Table 1), also known as GenX for its trade name, is one of per- and polyfluoroether carboxylic acid (PFECA) which has ether group in the middle of the carbon chain. It is applied as an alternative to the use of PFOA as a processing agent in the production of fluoropolymers (ECHA, 2015). However, its adverse effects on the liver, development, blood, and immune systems in rats or mice were observed with its lowest observed adverse effect level (LOAEL) at 0.5 mg/kg/day (USEPA, 2021). Gomis et al. (2018) reported that GenX had a higher toxicity ranking than PFOA when using modeled serum and liver, indicating that GenX had similar or higher

toxic potency.

Despite its toxic potential, the current production of GenX in Europe is estimated to be 10 to 100 tons/year (Vakili et al., 2021). Since its massive usage by many manufacturers, GenX has been detected in different water bodies in some countries, indicating its ubiquitous contamination worldwide (Table 2). Even worse, GenX is persistent against both conventional and advanced drinking water treatment processes (e.g., coagulation, flocculation, sedimentation, filtration, ozonation, and chlorination), despite being found in the source water of a water treatment plant up to 4,560 ng/L (Hopkins et al., 2018; Sun et al., 2016). Accordingly, the appropriate treatment of GenX in water is necessary.

Table 1. Physical and chemical properties of GenX (USEPA, 2021).

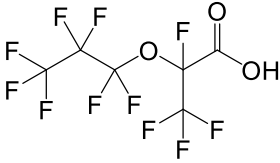
GenX (HFPO-DA)	Chemical formula	Molecular weight	pK _a	Water solubility
	C ₆ HF ₁₁ O ₃	330.06 g/mol	2.84 at 20 °C	>751 g/L at 20 °C

Table 2. Detection cases of GenX in different water matrices in various countries.

Location	Matrix	Concentration (ng L ⁻¹)	References
United States	River water	ND ~ 227	(Galloway et al., 2020)
	Drinking water	ND ~ <10	
Netherlands	River water	<0.2 ~ 812	(Gebbinck et al., 2017)
	Drinking water	<0.2 ~ 11	
China	River water	ND ~ 3060	(Heydebreck et al., 2015)
Netherlands	River water	ND ~ 86.08	
China	River water	0.78 ~ 2.49	(Pan et al., 2018)
German, Netherlands	River water	<0.05 ~ 10.3	
South Korea	River water	0.78 ~ 8.75	(Pan et al., 2018)
United Kingdom	River water	0.70 ~ 1.58	
United States	River water	0.59 ~ 1.98	(Pan et al., 2018)
China	Lake water	0.38 ~ 143.7	
Sweden	Lake water	0.88 ~ 2.68	(Sun et al., 2016)
United States	Source water of drinking water treatment plant (DWTP)	<10 ~ 4560	

1.2. Previous studies on the degradation of GenX

Several studies have been attempted to remove GenX in water using adsorption, advanced oxidation processes (AOPs), and advanced reduction processes (ARPs). The adsorption processes using activated carbon, ion-exchange resins, and membrane filtration processes can remove GenX, but do not destructively decompose it (Dixit et al., 2020; Wang et al., 2019a). This makes the adsorption process require treatment and management for the spent adsorbent, and filtration process create concentrated high-concentration wastewater (Vakili et al., 2021). Therefore, destructive treatments are desirable to prevent release into the environment (Pica et al., 2019).

AOPs including photochemical AOPs with UV irradiation are widely applied to decompose and remove micropollutants, in which strong oxidizing species such as hydroxyl radicals ($\bullet\text{OH}$) and sulfate radicals ($\text{SO}_4^{\bullet-}$) are active. However, $\bullet\text{OH}$ cannot achieve direct decomposition of GenX (Olvera-Vargas et al., 2022; Suresh Babu et al., 2022), and as shown in Table 3, $\text{SO}_4^{\bullet-}$ is reported to be ineffective for GenX removal due to steric hindrance by $-\text{CF}_3$ branch bound to α -carbon (Bao et al., 2018).

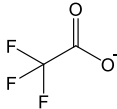
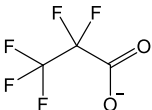
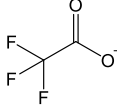
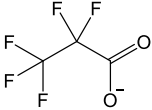
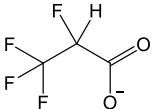
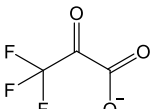
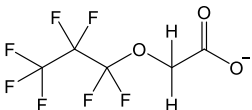
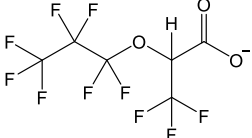
On the other hand, ARPs using hydrated electrons (e_{aq}^-) generated by the photolysis of inorganic reductive agents are emerging in the treatment of PFASs (Bao et al., 2019; Bentel et al., 2019; Cui et al., 2020; Song et al., 2013). Among them, UV/sulfite process of adding sulfite (SO_3^{2-}) with a high yield of e_{aq}^- has been recently studied for GenX (Eq. (1), Table 3) (Bao et al., 2018; Bentel et al., 2020b). Although

the removal rate differed depending on the experimental conditions of the two studies, both achieved efficient degradation of GenX and observed defluorination. The transformation products (TPs) identified in these studies are also shown in Table 3. Bao et al. (2018) identified TFA and PFPrA as TPs, which have standard reagents for target analysis, and Bentel et al. (2020b) further identified TPs through non-target analysis.



Still there are no researches on the effect of SO_3^{2-} ions on TP formation of GenX, further identification of TPs by a non-targeted analytical method in consideration of sulfonated-TPs is required to better understand the degradation mechanisms of GenX during the sulfite-based ARPs.

Table 3. Previous studies on the degradation of GenX during photochemical AOP and ARP.

Treatments	Removal	Defluorination	Identified TPs	References
UV	<5% (3 hr)	-	N/A	(Bao et al., 2018)
UV/persulfate (AOP)	<5% (3 hr)	-	N/A	(Bao et al., 2018)
UV/sulfite (ARP)	100% (2 hr)	90% (6 hr)	TFA  PFPrA 	(Bao et al., 2018)
UV/sulfite (ARP)	100% (48 hr)	45% (48 hr)	TFA  PFPrA     	(Bentel et al., 2020b)

1.3. Vacuum ultraviolet (VUV) studies on the degradation of micropollutants

Instead of applying UV that emits light with only 254 nm wavelength, applying the vacuum ultraviolet (VUV) as a light source that emits light with wavelengths of 185 nm and 254 nm can utilize both wavelengths of light. Therefore, VUV treatment process has been proposed as a more efficient alternative to the UV-based system (Zoschke et al., 2014). VUV radiation with 185 nm wavelength can generate high-energy photons (647 kJ/mol) sufficient for the cleavage of C-C (347 kJ/mol) and C-F (552 kJ/mol) bonds (Giri et al., 2012). This can result in the *in-situ* generation of reactive species such as e_{aq}^- , hydrogen atoms ($\bullet H$), and hydroxyl radicals ($\bullet OH$) via water homolysis (Eq. (2)) and ionization (Eq. (3)) (Gonzalez et al., 2004). Thus, micropollutants can be decomposed by VUV irradiation without adding additional chemicals. (Banayan Esfahani and Mohseni, 2022; Jin and Zhang, 2015; Kiattisaksiri et al., 2016; Wang and Zhang, 2014; Wu et al., 2020).



To our knowledge, there is no kinetic and mechanism study to decompose GenX in water during the VUV photolysis and VUV/sulfite reactions using VUV as a light source instead of UV. Especially, the studies on the identification of reactive species contribution such as e_{aq}^- and $\bullet H$, and the TPs during two reactions have not been studied yet.

1.4. Objectives

The objectives of this study are (1) to evaluate the degradation kinetics and mechanism including defluorination efficiency of GenX in water during VUV photolysis and VUV/sulfite processes; (2) to distinguish the contributions of various reactive species (e.g., e_{aq}^- , $\bullet H$, $\bullet OH$) during two processes; (3) to identify TPs during VUV photolysis and VUV/sulfite processes, and propose degradation pathways based on the identified TPs and density functional theory (DFT); and finally (4) to assess the toxicity of GenX and its TPs using ECOSAR and T.E.S.T simulation.

2. Materials and Methods

2.1. Chemicals

HFPO-DA ($\text{CF}_3\text{CF}_2\text{CF}_2\text{OCF}(\text{CF}_3)\text{COOH}$, 99%), also referred to as GenX, was purchased from Angene Chemical (Hong Kong, China). Trifluoroacetic acid (TFA, CF_3COOH), pentafluoropropionic acid (PFPrA, $\text{CF}_3\text{CF}_2\text{COOH}$), sodium sulfite, tert-butanol, sodium nitrite, sodium nitrate, ammonium acetate, and ammonium formate were purchased from Sigma-Aldrich (St. Louis, MO, USA). For pH adjustment, acetic acid, sodium acetate, sodium phosphate dibasic, sodium phosphate monobasic dihydrate, sodium tetraborate decahydrate, sodium hydroxide, and sulfuric acid were also purchased from Sigma-Aldrich (St. Louis, MO, USA). LC-MS grade methanol and acetonitrile were purchased from Thermo Fisher Scientific (Waltham, MA, USA). Deionized water was generated from Milli-Q deionized water generator (Millipore, MA, USA) and ultrapure nitrogen gas (N_2) was obtained from Daehangas (Gimpo, Korea) to purge oxygen in the reaction solution.

2.2. Experimental methods

All experiments were conducted in a batch-type photoreactor equipped with three 6-W low-pressure VUV mercury lamps (Sankyo Electric Co., Tokyo, Japan) emitting both VUV (185 nm) and UVC (254 nm) light (Fig. 1). The lamps were ignited for at least 10 min before the start of the experiments. The 2 L solution in the reactor was purged with nitrogen gas (N₂) continuously from 30 min before the start of all experiments to maintain a stable oxygen-free condition. Since laboratory-scale chemical experiments are performed under almost completely controlled conditions, experiments with small experimental errors were performed in duplicate, and experiments with relatively large experimental errors (in the case when standard deviations for $[C_t]/[C_0]$ were over 10%) were performed in triplicate to increase reliability.

To investigate the kinetics of GenX degradation, control tests were conducted under dark control, sulfite only, VUV photolysis, and VUV/sulfite processes. The effects of sulfite (SO₃⁻) concentration and pH on GenX degradation were examined using various sulfite concentrations (0-12 mM) and pHs (pH 4 to 10). The pH of the reaction solution was adjusted and buffered with 10 mM acetate buffer for pH 4, 10 mM phosphate buffer for pH 6-8, and 5 mM tetraborate buffer for pH 10. To compare the contributions of the reactive species, *tert*-butanol (*t*-BuOH), nitrite (NO₂⁻), and nitrate (NO₃⁻) ions were added as reactive species scavengers at 1 mM in the VUV photolysis system and at 6 mM in the VUV/sulfite system.

To identify the TPs and evaluate the defluorination efficiency during the

reactions, the initial concentration of GenX was set at 3.0 μM to identify the peaks of TPs produced and enable the quantification of fluoride ion (F^-) more clearly. In addition, no buffer was used to prevent the potential occurrence of any reaction between buffer chemicals and reactive species. Instead, the initial pH was adjusted by 1 M NaOH and H_2SO_4 .

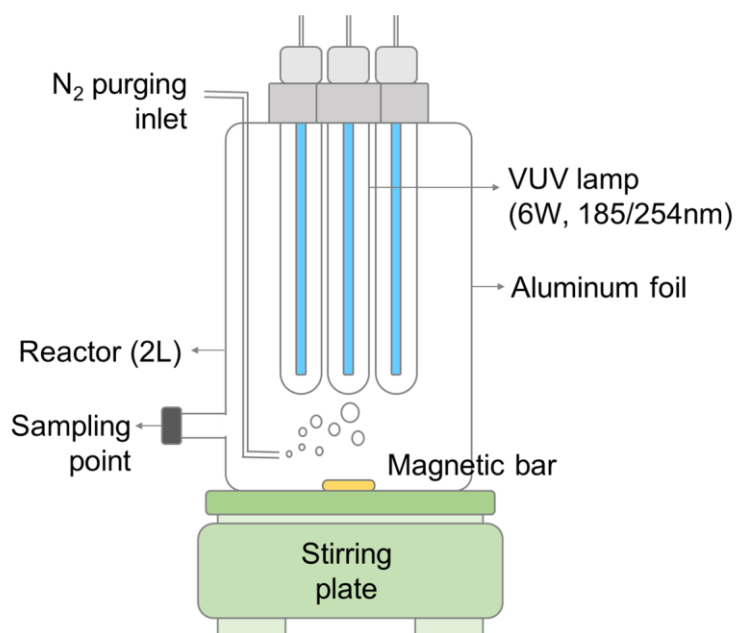


Fig. 1. Schematic diagram of the VUV reactor system.

2.3. Analytical methods

GenX was analyzed by high-performance liquid chromatography (HPLC-MS/MS) (Nexera, Shimadzu, Japan)-tandem mass spectrometer (API 4000, AB Sciex, USA) equipped with Gemini C18 column (2×50 mm, $3 \mu\text{m}$). The detailed analysis conditions are provided in Table S1 in the Supporting Information. TFA and PFPrA were also analyzed by using HPLC-MS/MS equipped with Raptor Polar X column (2.1×50 mm, $2.7 \mu\text{m}$). The detailed analysis conditions are provided in Table S2.

The identification of TPs during VUV photolysis and VUV/sulfite was determined by ultra-high performance liquid chromatography quadrupole time-of-flight mass spectrometry (UPLC-QTOF/MS) (Acquity UPLC Synapt G2-Si, Waters, USA) equipped with ACQUITY UPLC BEH C18 column (2.1×100 mm, $1.7 \mu\text{m}$). The detailed analysis conditions are provided in Table S3.

The ion selective electrode (ISE) (Thermo Scientific) connected to a Thermo Scientific Orion Versa Star Pro meter was used to determine the concentration of fluoride ions (F^-) (Scientific, 2016). The sample was added with the same amount of low-level TISAB solution, and the probe was immersed in the stirred solution. The probe was calibrated before each use with known concentrations of fluorine standard solutions.

2.4. Computational methods

DFT-based quantum chemical calculations were conducted with Gaussian 09 software (Frisch et al., 2016). The structural optimization and vibrational frequency calculations on GenX were preceded using B3LYP method with the 6-311+G (d,p) basis set including empirical dispersion GD3BJ (Bao et al., 2018). The solvent effects were also considered using the integral equation formalism variant (IEFPCM) (Tomasi et al., 1991).

To further determine the reactivity of GenX to the attack of reactive species at the atomic level, the condensed Fukui indices (f^+) based on condensed Fukui function and lowest unoccupied molecular orbital (LUMO) composition were calculated using Multiwfn 3.8 software, and visualized in GaussView 5.0.8 (Lu, 2014; Lu and Chen, 2012). Hirshfeld atomic charge and Hirshfeld partition were applied to the calculations. In addition, the Mayer bond order (BO) was calculated to find out which bonds are more likely to dissociate after being attacked by reactive species.

2.5. *In silico* toxicity assessment

The Ecological Structure Activity Relationships (ECOSAR v2.2) program was used to predict the acute and chronic toxicity of GenX and its identified TPs to aquatic organisms such as fish, *Daphnid*, and algae (USEPA, 2022a; b). The median lethal concentration (LC₅₀) and median effective concentration (EC₅₀) were estimated for acute toxicity. The chronic value (ChV) defined as the geometric mean of the no observed effect concentration (NOEC) and the lowest observed effect concentration (LOEC) was estimated for chronic toxicity.

The Toxicity Estimation Software Tool (T.E.S.T v5.1.2) was also used to predict the acute toxicity, bioconcentration factor, developmental toxicity and the Ames mutagenicity of GenX and its identified TPs (USEPA, 2020). The median lethal concentration (LC₅₀) and median lethal dose (LD₅₀) were estimated for acute toxicity to fathead minnow, *Daphnid*, and rat. The median growth inhibition concentration (IGC₅₀) for *T. pyriformis* was excluded since it was simulated as ‘not applicable (N/A)’ for all substances. The Consensus method was applied, which is recommended since it provided the most accurate predictions.

3. Results and Discussion

3.1. Degradation kinetics of GenX

Fig. 2 shows the degradation kinetics of GenX in dark control, sulfite only, VUV photolysis, and VUV/sulfite reactions at pH 10 under anoxic condition. While there was no degradation of GenX under dark control and sulfite-only conditions, approximately 35% of GenX removal in 3 hr was achieved with VUV photolysis reaction. This result indicates that the reactive species, such as e_{aq}^- , $\bullet H$, and $\bullet OH$, generated by the VUV photolysis of water could degrade GenX (Eq. (2) and Eq. (3)). When sulfite was added, the observed rate constant (k_{obs}) of GenX degradation increased by five times compared to the VUV photolysis reaction, achieving about 90% removal in 3 hr (Table S4). This is due to the additional generation of e_{aq}^- by the photolysis of sulfite (Eq. (1)), indicating that sulfite is an effective mediator at high solution pH.

We investigated the effect of sulfite concentration on the degradation of GenX during the VUV/sulfite process. As shown in Fig. 3, the degradation rate of GenX increased as the sulfite dosage increased up to 12 mM. This is attributed that as the concentration of sulfite increases, the generation of e_{aq}^- increases, resulting in a positive correlation (Song et al., 2013). However, the rate of increase showed a different pattern at low concentration levels (0-0.8 mM) and high concentration levels (2.4-12 mM). The excessive amount of sulfite did not significantly increase GenX degradation due to recombination and self-scavenging reaction between

reactive species such as $\text{SO}_3^{\cdot-}$ and e_{aq}^- (Eq. (4)-(6)) (Fischer and Warneck, 1996).



The ingestion of high concentrations of sulfite can also be a safety concern for human health (Han et al., 2020), and sulfite in water can be oxidized to sulfate in the presence of oxygen. Sulfate can naturally occur in drinking water, but intake of high concentrations by those not used to consuming sulfate can result in health effects such as dehydration and diarrhea (USEPA, 1999). Therefore, the addition of an excessively high concentration of sulfite to increase the removal efficiency of GenX should be avoided, and it is necessary to designate an appropriate concentration considering the health effects. In this study, other experiments for the kinetics of VUV/sulfite reaction were performed using 4.8 mM sulfite as the appropriate concentration.

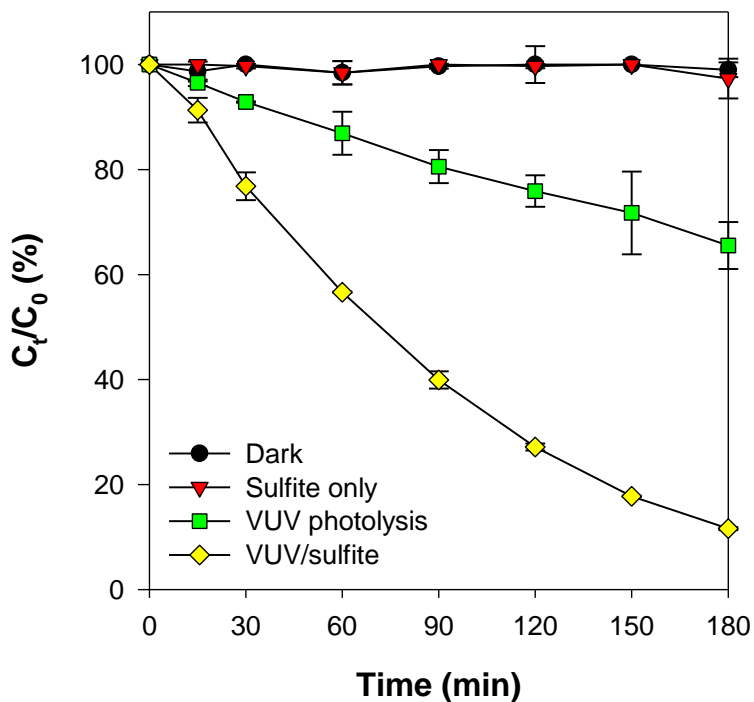


Fig. 2. Degradation of GenX during control tests for VUV/sulfite process under anoxic alkaline condition ($[\text{GenX}]_0 = 0.30 \mu\text{M}$, $[\text{sulfite}]_0 = 4.8 \text{ mM}$, $\text{pH} = 10$, VUV intensity_{254 nm} = 0.65 mW/cm^2 , continuous N_2 purging; $n \geq 2$).

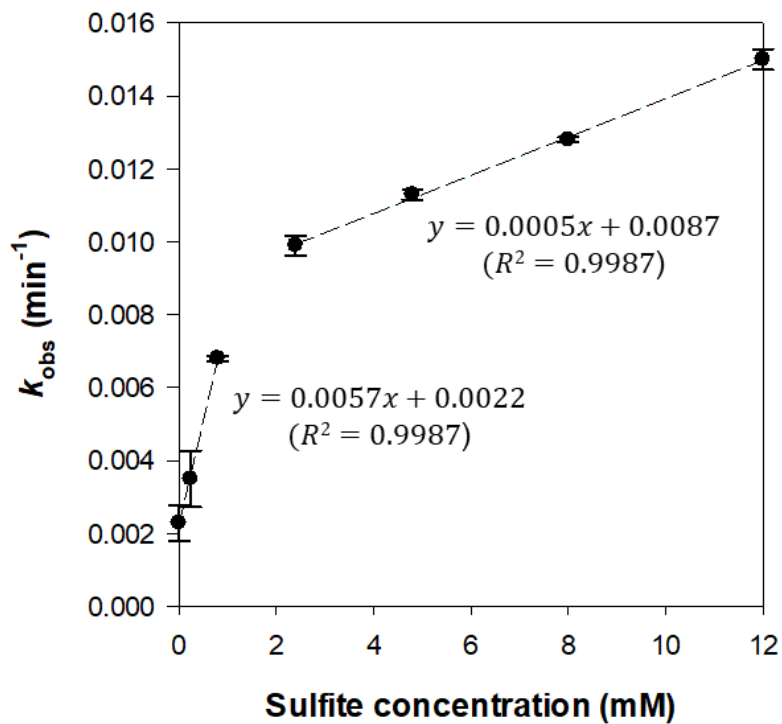


Fig. 3. Positive linear correlation with different slopes for pseudo-rate constants of GenX degradation as a function of sulfite concentration during VUV/sulfite process ($[\text{GenX}]_0 = 0.30 \mu\text{M}$, $\text{pH} = 10$, $\text{VUV intensity}_{254 \text{ nm}} = 0.65 \text{ mW/cm}^2$, continuous N_2 purging, $n \geq 2$).

3.2. Effect of pH

The rate constants for the degradation of GenX under various pH conditions during VUV photolysis and VUV/sulfite reactions were shown in Fig. 4. In VUV/sulfite reaction, the degradation rate increased as the pH increased. This is because the higher concentration of e_{aq}^- is produced due to the dominant form of sulfite (SO_3^{2-}) ($pK_a = 7.21$) among S(IV) species (Gu et al., 2017) (Fig. S1), the donor of e_{aq}^- , at alkaline conditions (Eq. (1)). Also, under acidic condition, e_{aq}^- can react with H^+ to form $\bullet H$ (Eq. (7)), whereas $\bullet H$ can react with OH^- to form e_{aq}^- under alkaline condition (Eq. (8)) (Fischer and Warneck, 1996).



Unlike the VUV/sulfite reaction, the fastest GenX degradation was observed at pH 6 during the VUV photolysis reaction, followed by pH 4, pH 8, and pH 10. While $\bullet OH$ is known to be ineffective for GenX degradation (Bao et al., 2018; Ding et al., 2022), the two reactive species, e_{aq}^- and $\bullet H$, differ in pH conditions for each to be effectively produced, according to aforementioned reactions (Eq. (7) and Eq. (8)). If the $\bullet H$ acts predominantly, the lower pH would have better removal efficiency. Conversely, if the e_{aq}^- acts predominantly, the higher pH would be better for GenX removal. However, the result that the optimum pH was not biased toward either strong acid or strong base demonstrates that e_{aq}^- and $\bullet H$ were both utilized in GenX degradation during the VUV photolysis reaction. This result seems plausible because

the quantum yield of $\bullet\text{H}$ is much higher than that of e_{aq}^- in the VUV photolysis reaction (Eq. (2) and Eq. (3)), and $\bullet\text{H}$ can cleave the C-C bonds with a lower but still high reduction potential than e_{aq}^- (Qu et al., 2014). This was also confirmed by the change of pH during the experiment for 6 hr without using a buffer solution (Fig. 5). The solution pH decreased after the VUV photolysis reaction, we inferred that $\bullet\text{H}$ reacted with GenX by providing an electron and was converted into H^+ .

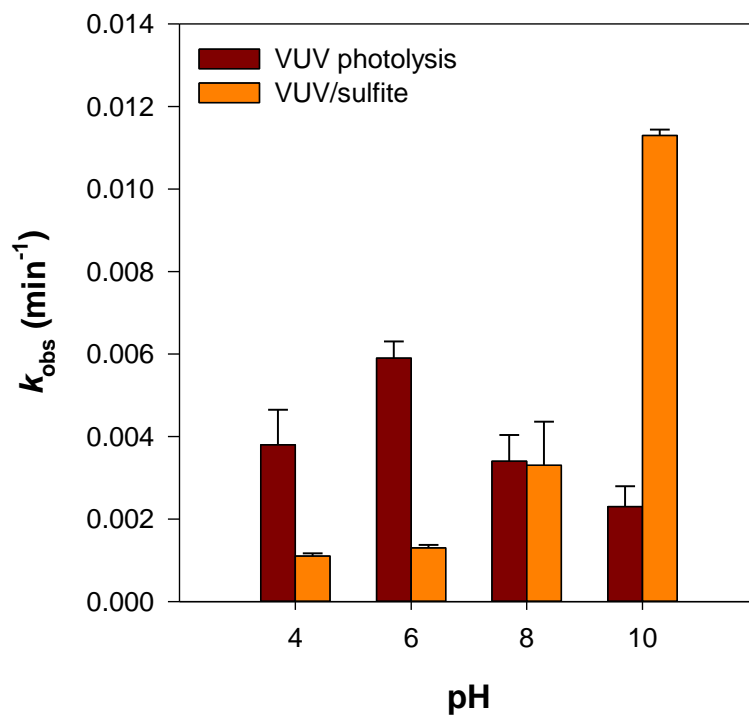


Fig. 4. Degradation kinetics of GenX at different pH during VUV photolysis and VUV/sulfite ($[\text{sulfite}]_0 = 4.8 \text{ mM}$) processes ($[\text{GenX}]_0 = 3.0 \text{ }\mu\text{M}$, VUV intensity_{254 nm} = 0.65 mW/cm^2 , continuous N₂ purging, $n \geq 2$).

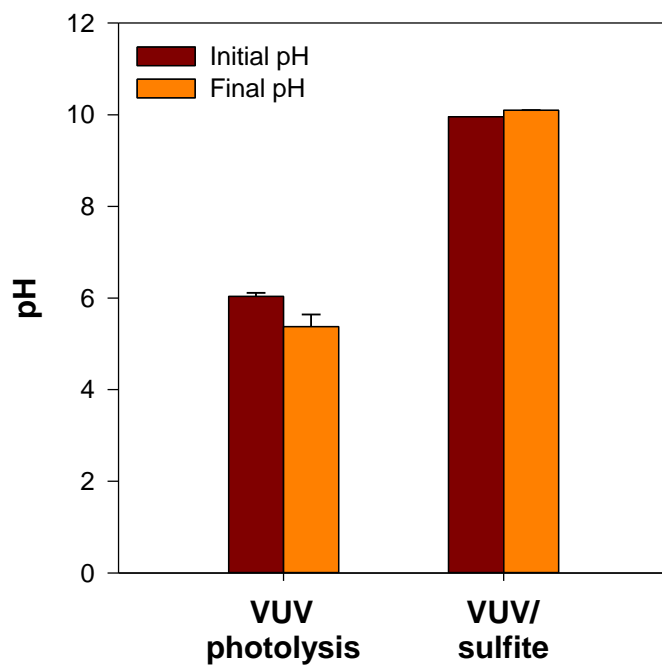
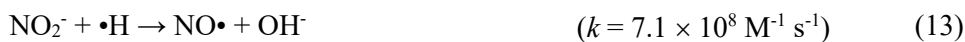
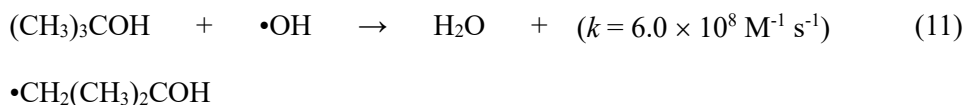


Fig. 5. The change of pH after degradation for 6 h in VUV photolysis ($\text{pH}_0 = 6$) and VUV/sulfite ($\text{pH}_0 = 10$) processes without using buffer solution.

3.3. Roles of reactive species

To explore the roles of reactive species (e.g., e_{aq}^- , $\bullet H$, $\bullet OH$) in GenX degradation, the experiments were conducted by adding scavengers including *t*-BuOH, NO_2^- , and NO_3^- ions. The second-order rate constants between each scavenger and reactive species are presented in Eq. (9)-(16) (Buxton et al., 1988; NIST, 2022).



As shown in Fig. 6, the change in the rate constant is clear when each scavenger was added. When *t*-BuOH was present, there was no significant change in the rate constant in the VUV photolysis reaction, whereas the rate constant significantly increased during the VUV/sulfite reaction. While *t*-BuOH is a powerful scavenger for $\bullet OH$ (Eq. (11)), it has a relatively small scavenging effect on e_{aq}^- and $\bullet H$, which can be negligible (Eq. (9) and Eq. (10)). This result implies that $\bullet OH$

played a negligible role in GenX degradation during the VUV photolysis reaction, and even showed a significantly negative effect during the VUV/sulfite reaction. It is reported that $\bullet\text{OH}$ reacts with e_{aq}^- and $\bullet\text{H}$ to quench these two reductive reactive species (Eq. (17)-(18)) (Buxton et al., 1988; Kim et al., 2022). This quenching effect was minimal in the VUV photolysis reaction and was huge in the VUV/sulfite reaction because the amount of e_{aq}^- that reacted with $\bullet\text{OH}$ increased as a large amount of e_{aq}^- was generated by the photolysis of sulfite.



To compare the contribution of e_{aq}^- and $\bullet\text{H}$ during the reactions, NO_2^- and NO_3^- ions were used as scavengers. While both are good scavengers for e_{aq}^- , only NO_2^- can react rapidly with $\bullet\text{H}$ and $\bullet\text{OH}$ (Eq. (12)-(16)). When NO_2^- and NO_3^- ions were added, significant inhibition of GenX degradation in VUV photolysis and VUV/sulfite reactions was observed, indicating that either e_{aq}^- or $\bullet\text{H}$, or both played a dominant role in both reactions (Fig. 6). Note that, from the experiments of pH effect, it is known that not only e_{aq}^- but also $\bullet\text{H}$ contributes in the VUV photolysis reaction, and that e_{aq}^- has a significantly dominant contribution in the VUV/sulfite reaction.

Slightly higher inhibition of GenX decomposition was observed when NO_3^- ion was added than when NO_2^- ion was added even though NO_2^- reacts with $\bullet\text{H}$ about 500 times faster than NO_3^- (Eq. (13) and Eq. (16)), it is presumed to be due to the scavenging effect for $\bullet\text{OH}$ by NO_2^- ions. Unlike the case where *t*-BuOH was added and e_{aq}^- and $\bullet\text{H}$ were sufficient similar to the control test, the quenching effects for

these two by $\bullet\text{OH}$ (Eq. (17) and Eq. (18)) were relatively increased since the amount of e_{aq}^- and $\bullet\text{H}$ produced was insufficient when NO_3^- ions were present.

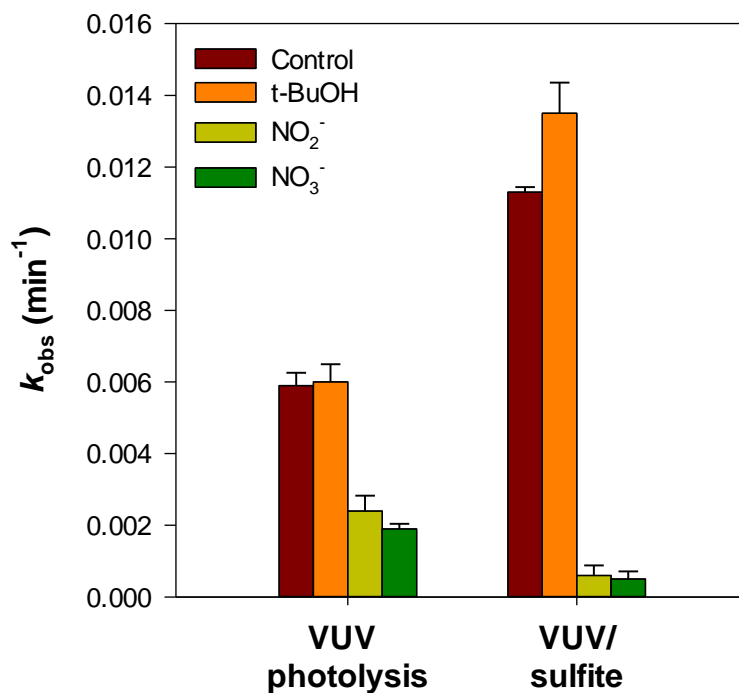


Fig. 6. Pseudo-first rate constants of GenX degradation in the absence or presence of different radical scavengers during VUV photolysis ($[\text{t-BuOH}] = [\text{NO}_2^-] = [\text{NO}_3^-] = 1 \text{ mM}$, $\text{pH} = 6$) and VUV/sulfite ($[\text{sulfite}]_0 = 4.8 \text{ mM}$, $[\text{t-BuOH}] = [\text{NO}_2^-] = [\text{NO}_3^-] = 6 \text{ mM}$, $\text{pH} = 10$) processes ($[\text{GenX}]_0 = 0.30 \text{ }\mu\text{M}$, $\text{VUV intensity}_{254 \text{ nm}} = 0.65 \text{ mW/cm}^2$, continuous N_2 purging, $n \geq 2$).

3.4. Identified TPs and defluorination

To propose a possible degradation pathway through VUV photolysis and VUV/sulfite processes, quantitative and qualitative analyses of TPs were conducted. The non-targeted qualitative analysis data analyzed by LC-QTOF/MS went through the suspect screening process using UNIFI software (Waters, USA). The expected TPs list for suspect screening was drawn using ChemDraw 20.0 software, including various substances that may occur due to reaction mechanisms such as C-O bond breakage and H/F exchange. Among the substance identified through the screening process, substances that met the following criteria were defined as TPs: (i) mass error < 10 ppm; (ii) isotope match intensity RMS percent < 20%; (iii) peak area showing a continuous pattern over time, such as steady increase or a decrease after increase.

The time profiles of ultra-short chain PFASs (TFA and PFPrA) subjected to target analysis using LC-MS/MS are shown in Fig. 7(a) and Fig. 7(c) with defluorination efficiency, and the time profiles of the other TPs (TP120, TP164, TP182, TP186, and TP366) subjected to non-target analysis using LC-QTOF/MS are shown in Fig. 7(b) and Fig. 7(d).

During the VUV photolysis reaction, while both PFPrA and TFA were detected by target analysis (Fig. 7(a)), TP120 and TP164 were detected by non-target analysis (Fig. 7(b), Table S5). It was confirmed that TP164 was the same compound as PFPrA, and TFA was difficult to detect via non-target analysis due to its small molecular weight. The defluorination efficiency defined by Eq. (19) showed 17% of fluorine

ion (F⁻) conversion from GenX was achieved after 6 hr reaction (Fig. 7(a)). Although the VUV photolysis did not effectively break the C-F bonds of GenX, the result showed that some degree of defluorination can be achieved with reactive species only generated by photolysis of water without the addition of other chemicals.

$$\text{Defluorination efficiency (\%)} = \frac{\text{Observed concentration of F}^{-} \text{ (mg/L)}}{\text{Theoretical concentration of F}^{-} \text{ (mg/L)}} \times 100 \quad (19)$$

While TFA, PFPrA (TP164), and TP120 were found in the VUV photolysis reaction (Fig. 7(c)), three TPs (TP182, TP186, and TP366) were additionally identified during the VUV/sulfite reaction (Fig. 7(d), Table S5). Among them, the sulfonated TPs, which are TP182 and TP366, are newly identified in this study, and the other four TPs (TFA, PFPrA (TP164), TP120, and TP186) were the same as the existing literature in which the decomposition of GenX by that the ether group bond is broken (Bao et al., 2018; Bentel et al., 2020b; Trang et al., 2022). The achievement of 67% F⁻ conversion during the VUV/sulfite reaction indicated that the generation of additional e_{aq}⁻ by the photolysis of sulfite (Eq. (1)) enhanced the defluorination efficiency of GenX.

To determine the existence of unidentified TPs, the mass balances of fluorine (F) were calculated from the quantification result of target TPs and F⁻ in Fig. 7(a) and Fig. 7(c). The ratio of the total fluorine contained in remaining GenX, PFPrA, TFA, and F⁻ was calculated through Eq. (20).

$$\text{Fluorine recovery (\%)} = \frac{([\text{GenX}] \times 11) + ([\text{PFPrA}] \times 5) + ([\text{TFA}] \times 3) + [\text{F}^{-}]}{[\text{GenX}]_0 \times 11} \times 100 \quad (20)$$

As shown in Fig. 8, fluorine recovery decreased to 54% after 6 hr in the VUV photolysis reaction, while it decreased to 46% by 120 min and finally increased to 68% in the VUV/sulfite reaction. The missing recovery of fluorine indicates the presence of unquantified or unidentified TPs. In particular, the decrease of TP120 after 150 min, the only unquantified among the identified TPs in the VUV photolysis reaction, did not lead to an increase in fluorine recovery, suggesting the existence of unidentified TPs with fluorine. In contrast, the increase in the recovery after 120 min during the VUV/sulfite reaction indicates that the decomposition and defluorination of unquantified TPs had progressed.

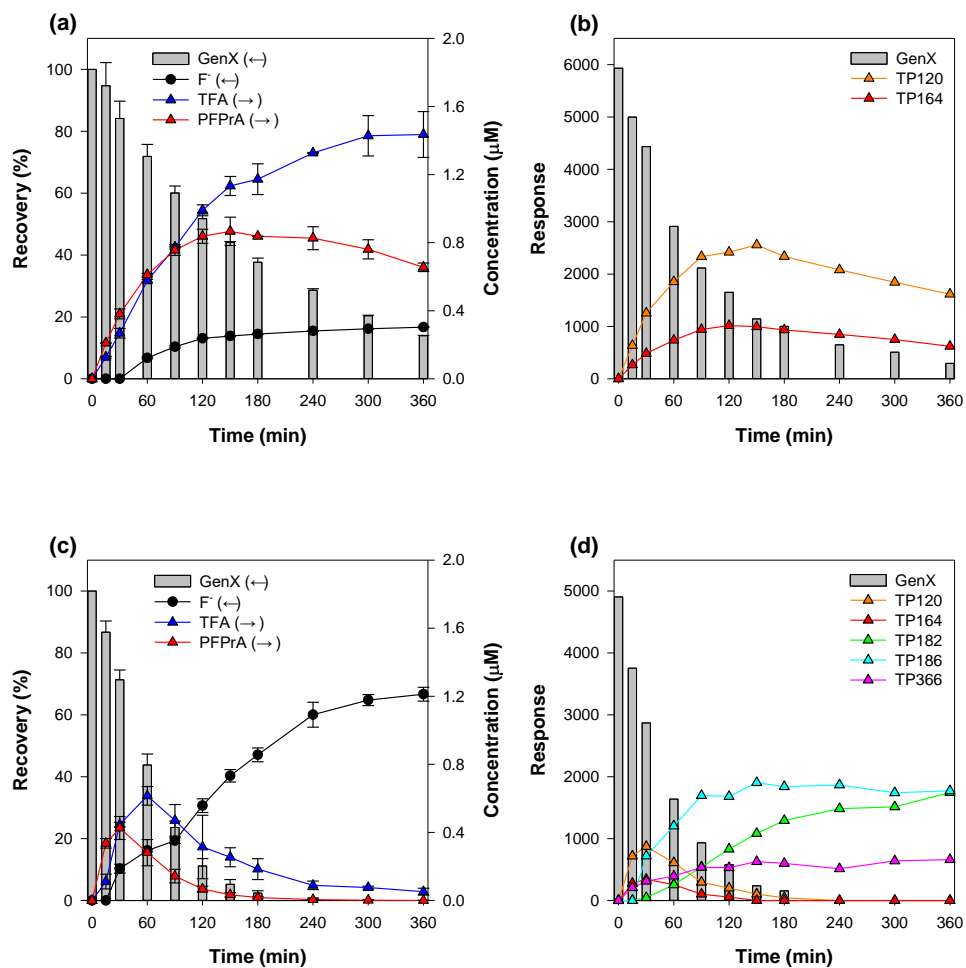


Fig. 7. Time profiles for the response of identified TPs using (a) LC-MS/MS, (b) LC-QTOF/MS during VUV photolysis (pH = 6), and (c) LC-MS/MS, (d) LC-QTOF/MS during VUV/sulfite ($[\text{sulfite}]_0 = 8.0 \text{ mM}$, pH = 10) processes ($[\text{GenX}]_0 = 3.0 \text{ } \mu\text{M}$, VUV intensity_{254 nm} = 0.65 mW/cm², continuous N₂ purging; n = 2).

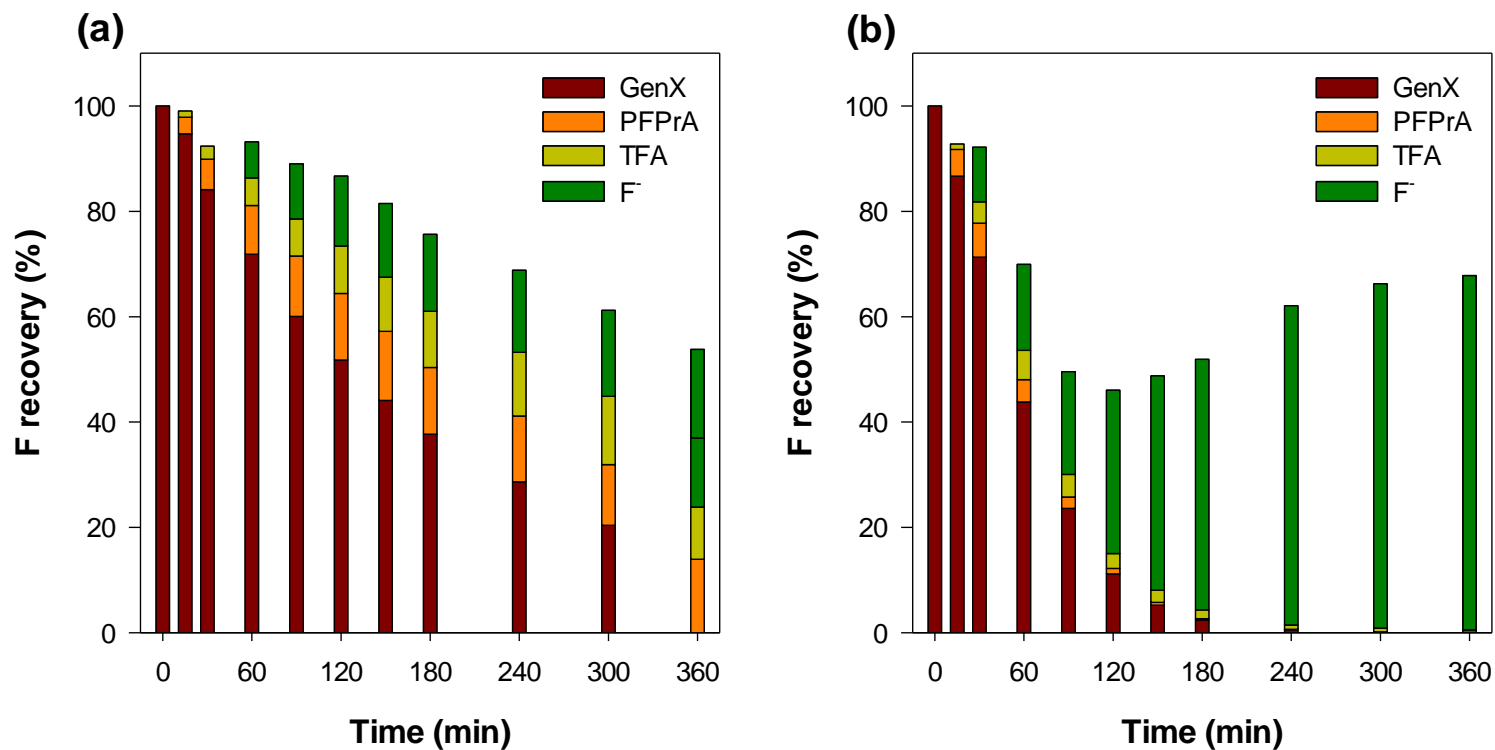


Fig. 8. Mass balance of fluorine during (a) VUV photolysis (pH = 6) and (b) VUV/sulfite ($[\text{sulfite}]_0 = 8.0 \text{ mM}$, pH = 10) processes ($[\text{GenX}]_0 = 3.0 \text{ }\mu\text{M}$, VUV intensity_{254 nm} = 0.65 mW/cm², continuous N₂ purging; n = 2).

3.5. Theoretical calculation and degradation mechanisms

Theoretical calculations were performed to deepen the perspective on the degradation mechanisms of GenX under the VUV-based reactions. As GenX exists in anion form in water at most pH values due to its low pK_a value ($pK_a = 2.84$ (USEPA, 2021)), the calculations were carried out using the anionic form of GenX to reflect the actual molecular state of GenX in the aqueous environment. The optimized geometric structure of GenX is shown in Fig. S2. The f^+ describes the susceptibility to nucleophilic attack at the atomic level based on electron density, and LUMO describes the ability to accept electrons at the molecular level based on the orbital. The positively larger the f^+ value, the easier it is to be subjected to nucleophilic attack. The contour surface for f^+ depicts that the CF_3 fragment and CF_2 fragment of nonionic moiety are the most preferable sites for nucleophilic attack (Fig. 9(a), Table 4). Moreover, the LUMO in the GenX molecule is distributed throughout the carbon chain including the functional group (Fig. 9(b)), which seems to be induced by a partial positive charge at the carbon atoms due to the relatively strong electronegativity of fluorine and oxygen atoms. Among them, atoms with high composition are found to be C(18) (13.509%), C(4) (10.311%), and C(2) (9.554%) (Table 5), which are likely to accept the electrons. Based on the computational calculations and identification of TPs, the proposed degradation pathways of GenX during VUV photolysis and VUV/sulfite reactions are shown in Fig. 10.

The initial reaction for GenX decomposition in the VUV/sulfite reaction can be proceeded into three pathways depending on in which site the chemical bond would be dissociated. First, $\bullet H$ and e_{aq}^- attacks C(2) of GenX to form TP120, PFPrA,

and TFA (Fig. 10). At this time, the attacked C(2) is the atom susceptible to nucleophilic attack in consideration of f^+ (Table 4), and this attack would lead to cleavage of the C(2)-C(3) bond, which has a lower bond order (BO) (-6.5335) than that of C(1)-C(2) bond (-0.6022) when an electron is added to GenX molecule (i.e., GenX⁻²⁻) (Table 6). This reaction can also occur in the VUV photolysis reaction. The difference is that not only e_{aq}^- but also $\bullet H$ can participate in this reaction during the VUV photolysis reaction whereas e_{aq}^- plays a predominant role in the VUV/sulfite reaction due to the less effective formation of $\bullet H$.

Among the two segments generated in this way as shown in Fig. 10, $CF_3CF_2\bullet$ can react with $\bullet H$ or H_2O to form TP120 (Eq. (21) and Eq. (22)), or reacts with $\bullet COO^-$ to form PFPrA (Eq. (23)) during both VUV photolysis and VUV/sulfite reactions. Considering the time profile for the response of these two TPs, it is inferred that the reaction which generates TP120 is the major reaction in the VUV photolysis reaction (Fig. 7(a) and Fig. 7(d)). On the other hand, the decarboxylated TP of GenX was not detected although the $\bullet COO^-$ used in the formation of PFPrA during the VUV photolysis and VUV/sulfite reactions is presumed to be from the functional group of GenX. As for TFA, the main source seems to be the other fragment ($\bullet CF_2OCF(CF_3)COO^-$) unlike TP120 and PFPrA. According to previous literatures, the amount of conversion from PFPrA to TFA was minimal during the destruction of PFPrA by the nucleophilic attack in UV/sulfite and solvolysis reactions. (Bentel et al., 2020a; Trang et al., 2022). Therefore, in order to explain the change in the concentration of TFA showing a similar pattern to PFPrA, it is reasonable to assume that the generated TFA is not converted from PFPrA (Fig. 7(a) and Fig. 7(d)).



In the second route, e_{aq}^- attacks C(4), the α -carbon in the ether group, and breaks the C-O bond. TP186 formed here was confirmed as the highest response value in the VUV/sulfite reaction, indicating that this reaction is the most major pathway in VUV/sulfite reaction (Eq. (24)). Lastly, the identification of TP366 implies the third route with cleavage of C(4)-C(18) bond by e_{aq}^- attack. After dissociation, the decarboxylated fragment ($\text{CF}_3\text{CF}_2\text{CF}_2\text{OCF}(\text{CF}_3)\bullet$) could react with SO_3^- to form sulfonated intermediates (Eq. (25)). Then, the C-O bond is broken due to the attack of e_{aq}^- analogous to the second route, forming TP182 in addition to TP186. This can be supported by other literatures that have found sulfonated TPs (Ren et al., 2021; Song et al., 2013).



All these results demonstrate that the reaction does not occur only at the most reactive site calculated by the Fukui function, but that the reaction can proceed in parallel at multiple sites. However, it is noteworthy that $\bullet\text{H}$ attack can occur at the site most reactive to nucleophilic attack, and this makes slower degradation and defluorination rates of GenX in VUV photolysis than VUV/sulfite process since the slower reaction rate of $\bullet\text{H}$ than that of e_{aq}^- .

Table 4. Calculated Hirshfeld charge and condensed Fukui index f^+ of each atom in GenX.

Atom	q(N+1)	q(N-1)	f^+
C(1)	0.2668	0.2692	0.0024
F(14)	-0.0921	-0.0882	0.0039
F(15)	-0.0905	-0.0877	0.0028
F(16)	-0.0906	-0.0879	0.0027
C(2)	0.1668	0.1709	0.0041
F(12)	-0.0931	-0.0872	0.0059
F(13)	-0.0936	-0.0877	0.0059
C(3)	0.2393	0.2502	0.0109
F(10)	-0.1118	-0.0979	0.0138
F(11)	-0.1064	-0.0929	0.0134
O(17)	-0.1453	-0.1208	0.0245
C(4)	0.1354	0.2053	0.0699
F(6)	-0.1371	-0.0819	0.0552
C(5)	0.2578	0.2752	0.0174
F(7)	-0.1037	-0.0799	0.0238
F(8)	-0.1137	-0.0832	0.0305
F(9)	-0.1045	-0.0837	0.0208
C(18)	0.0898	0.2087	0.1189
O(19)	-0.4382	-0.1984	0.2399
O(20)	-0.4354	-0.1020	0.3334

Table 5. The LUMO composition of GenX.

Atom	Composition (%)
C(1)	6.105
F(14)	5.775
F(15)	1.387
F(16)	0.977
C(2)	9.554
F(12)	7.197
F(13)	3.195
C(3)	6.346
F(10)	1.480
F(11)	1.413
O(17)	6.874
C(4)	10.311
F(6)	1.466
C(5)	3.707
F(7)	1.221
F(8)	1.439
F(9)	1.548
C(18)	13.509
O(19)	8.229
O(20)	8.266

Table 6. Mayer bond order value of GenX²⁻.

Bond	Bond order
C(1)-C(2)	-0.6022
C(1)-F(14)	0.8551
C(1)-F(15)	1.1083
C(1)-F(16)	1.1149
C(2)-C(3)	-6.5335
C(2)-F(12)	1.6636
C(2)-F(13)	1.6321
C(3)-F(10)	1.3015
C(3)-F(11)	1.4346
C(3)-O(17)	0.7712
C(4)-C(5)	1.1154
C(4)-F(6)	1.4949
C(4)-O(17)	1.1163
C(4)-C(18)	0.9184
C(5)-F(7)	1.1144
C(5)-F(8)	1.1169
C(5)-F(9)	1.0546
C(18)-O(19)	1.6111
C(18)-O(20)	1.6724

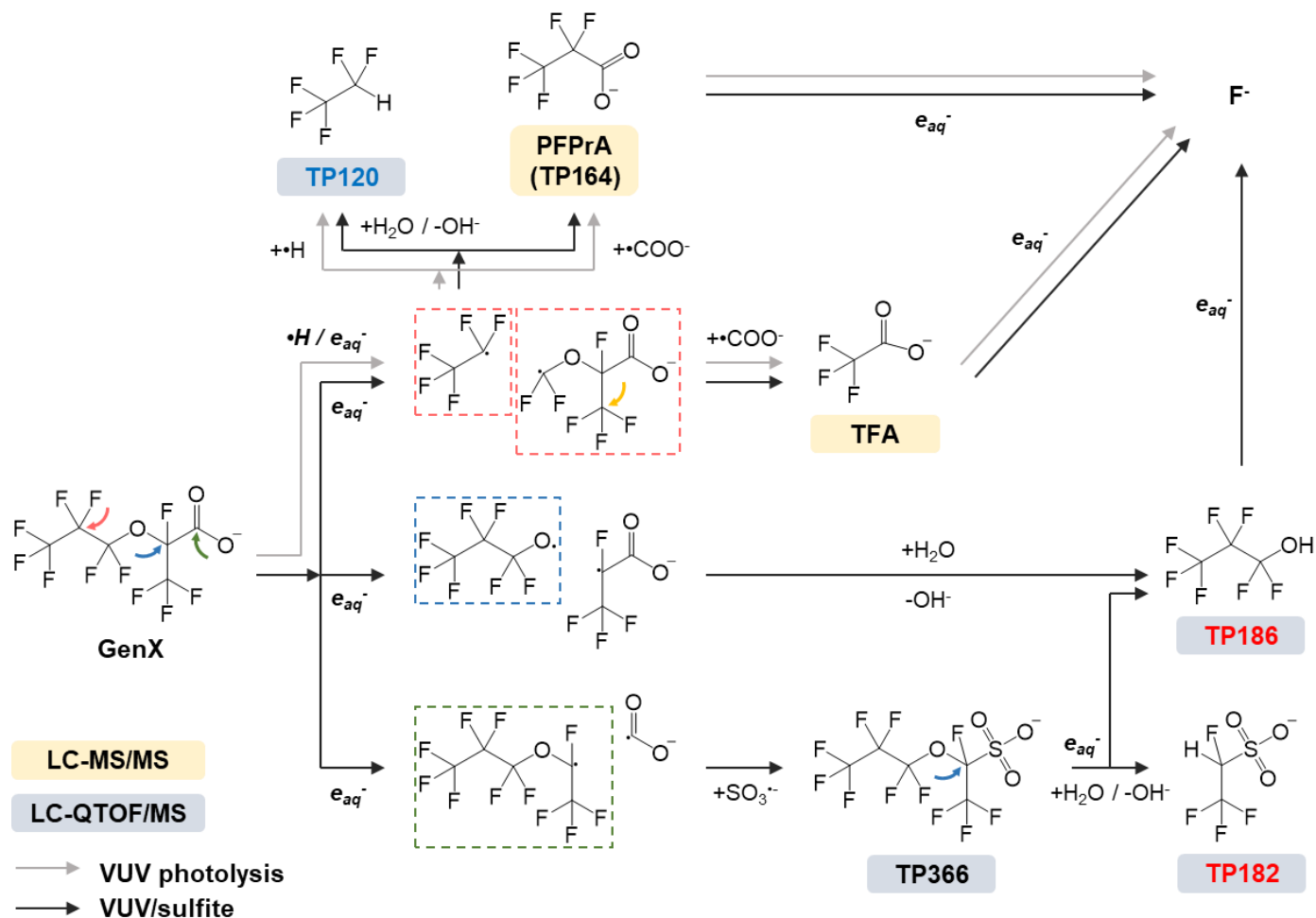


Fig. 10. Proposed degradation pathway of GenX in VUV photolysis and VUV/sulfite processes (blue and red texts correspond to the main TPs of VUV photolysis and VUV/sulfite processes, respectively).

3.6. *In silico* toxicity assessment

The acute and chronic toxicity of GenX and identified TPs during two VUV-based reactions were assessed to examine the change in ecotoxicity during the degradation of GenX using ECOSAR and T.E.S.T. software. The toxicity can be classified according to the Globally Harmonized System of Classification and Labeling of Chemicals (Table S6). The bioconcentration factor, developmental toxicity, and Ames mutagenicity were also predicted using T.E.S.T software.

The toxicity values predicted using ECOSAR simulation are shown in Table 7. The ECOSAR result showed that GenX itself did not show acute toxicity to fish, *Daphnid*, and green algae, but its chronic toxicity was rated as ‘harmful’ to all three species. When GenX was degraded through decarboxylation followed by sulfonation, as shown in Fig. 10, the generated TPs such as TP366 and TP182 during the VUV/sulfite reaction showed very low toxicity compared to the parent compound. Both PFPrA and TFA produced in both reactions, which are ultra-short chain PFASs, were also assessed to be ‘not harmful’ in both acute toxicity and chronic toxicity. However, TP120 and TP186 which are the TPs with H atoms attached after C-C bond cleavage and C-O bond cleavage, showed a ‘harmful’ level of chronic toxicity. In particular, TP120 showed even ‘harmful’ in acute toxicity to green algae with higher chronic toxicity than the parent compound.

The toxicity values predicted using T.E.S.T simulation are shown in Table 8. The T.E.S.T result determined that GenX was ‘harmful’ for acute toxicity, which is more sensitive than the ECOSAR result for *Daphnid*. In addition, acute toxicity to

fathead minnow or oral intake of rats, which is evaluated only in the T.E.S.T., showed that TP366 had the 'toxic' class for the former, and TPs except for TP186 had more than 'harmful' toxicity for the latter. Regarding developmental toxicity, four TPs (TP182, PFPrA, TP120, and TFA) appeared to be developmental toxicants, whereas five TPs with TP186 were negative for mutagenicity.

Taken together, GenX and its TPs can be harmful to the ecosystem and have developmental toxicity effects to humans or animals. In particular, the retention of TP366 after VUV/sulfite reaction and TFA after VUV photolysis reaction can lead to significantly increased acute toxicity for fathead minnow and oral intake of rats. Thus, the potential toxicity of the reductive decomposition of GenX should be reduced with longer reaction time or further effective removal strategies, and follow-up studies supporting the ecotoxicity change observed through experiments are required.

Table 7. Predicted toxicity for GenX and its TPs using ECOSAR simulation.

Compounds	Acute toxicity			Chronic toxicity		
	Fish	<i>Daphnid</i>	Algae	Fish	<i>Daphnid</i>	Algae
	LC ₅₀ (96 hr) (mg/L)	LC ₅₀ (48 hr) (mg/L)	EC ₅₀ (96 hr) (mg/L)	(mg/L)	(mg/L)	(mg/L)
GenX*	161.74	104.15	130.56	18.34	14.42	45.25
TP366**	1.53E+04	8.06E+03	4.45E+03	1.37E+03	642.06	990.83
TP186**	508.55	273.67	163.28	46.66	22.98	37.94
TP182**	1.34E+06	5.62E+05	1.19E+05	9.17E+04	2.36E+04	1.59E+04
PFPrA (TP164)*	4.04E+03	2.19E+03	1.33E+03	373.03	185.98	312.11
TP120*	251.49	136.95	85.82	23.40	11.89	20.48
TFA*	2.07E+04	1.02E+04	4.31E+03	1.72E+03	680.19	830.54

* : remaining after VUV photolysis reaction for 6 hr

** : remaining after VUV/sulfite reaction for 6 hr

Table 8. Predicted toxicity for GenX and its TPs using T.E.S.T simulation.

Compounds	Acute toxicity			Developmental toxicity	Ames mutagenicity
	Fathead minnow	<i>Daphnid</i>	Rat		
	LC ₅₀ (96 hr) (mg/L)	LC ₅₀ (48 hr) (mg/L)	LD ₅₀ (oral) (mg/kg)		
GenX*	22.26	61.27	722.14	N/A	N/A
TP366**	5.94	N/A	579.52	N/A	N/A
TP186**	123.84	203.69	3382.07	N/A	Negative
TP182**	121.92	N/A	698.39	Yes	Negative
PFPrA (TP164)*	244.71	244.60	628.68	Yes	Negative
TP120*	185.13	176.77	1626.19	Yes	Negative
TFA*	361.53	661.11	188.35	Yes	Negative

* : remaining after VUV photolysis reaction for 6 hr

** : remaining after VUV/sulfite reaction for 6 hr

4. Conclusions

In this study, we investigated the degradation kinetics and mechanisms of GenX during VUV photolysis and VUV/sulfite processes under anoxic condition. When using VUV instead of UV as the light source, it was confirmed that defluorination of GenX is possible not only when sulfite is added but also during photolysis due to the formation of e_{aq}^- and $\bullet H$. Because of the difference in the contribution of the active reactive species, VUV photolysis reaction has optimum efficiency at near-neutral pH, whereas VUV/sulfite reaction has optimum efficiency at the extreme condition of high pH. Thus VUV photolysis, which can be treated only with light sources without additional chemicals, can be applied to water treatment processes such as drinking water treatment, where the level of GenX is low, operation in extreme conditions is difficult, and the pH after treatment must be considered. On the other hand, in processes where oxygen in water is low and relatively high concentrations of GenX are likely to occur, such as wastewater treatment, it is necessary to maximize treatment efficiency by adding sulfite and increasing pH.

It was confirmed that C-C bond cleavage occurred in VUV photolysis reaction, and the observation of defluorination suggested that C-F bond cleavage also occurred. In VUV/sulfite reaction, it was confirmed that C-C bond cleavage and C-O bond cleavage occurred, and decarboxylation and C-F bond cleavage also occurred. Through these reactions, three TPs (TFA, PFPrA, and TP120) were identified to be produced in the VUV photolysis reaction and TP182, TP186, and TP266 were

additionally identified to be produced in the VUV/sulfite reaction. In particular, the residues of potentially toxic TPs such as TP120 and TP186 suggest that sufficient reaction time should be provided, or research to eliminate them needs to be continued.

Overall, the achievements of this study are (1) confirmation of efficient degradability of GenX through VUV photolysis and VUV/sulfite; (2) distinguishing which reactive species contribute to each process; (3) broadening the view for the degradation mechanism of GenX during VUV photolysis and VUV/sulfite processes based on identified TPs and DFT calculations; and (4) suggesting toxicity potential for TPs. These will provide scientific information for the establishment of a water treatment system to remove and mineralize GenX.

5. References

- Banayan Esfahani, E. and Mohseni, M. 2022. Fluence-based photo-reductive decomposition of PFAS using vacuum UV (VUV) irradiation: Effects of key parameters and decomposition mechanism. *Journal of Environmental Chemical Engineering* 10(1), 107050.
- Bao, Y., Deng, S., Jiang, X., Qu, Y., He, Y., Liu, L., Chai, Q., Mumtaz, M., Huang, J., Cagnetta, G. and Yu, G. 2018. Degradation of PFOA Substitute: GenX (HFPO–DA Ammonium Salt): Oxidation with UV/Persulfate or Reduction with UV/Sulfite? *Environmental Science & Technology* 52(20), 11728-11734.
- Bao, Y., Huang, J., Cagnetta, G. and Yu, G. 2019. Removal of F–53B as PFOS alternative in chrome plating wastewater by UV/Sulfite reduction. *Water Research* 163, 114907.
- Bentel, M.J., Liu, Z., Yu, Y., Gao, J., Men, Y. and Liu, J. 2020a. Enhanced Degradation of Perfluorocarboxylic Acids (PFCAs) by UV/Sulfite Treatment: Reaction Mechanisms and System Efficiencies at pH 12. *Environmental Science & Technology Letters* 7(5), 351-357.
- Bentel, M.J., Yu, Y., Xu, L., Kwon, H., Li, Z., Wong, B.M., Men, Y. and Liu, J. 2020b. Degradation of Perfluoroalkyl Ether Carboxylic Acids with Hydrated Electrons: Structure–Reactivity Relationships and Environmental Implications. *Environmental Science & Technology* 54(4), 2489-2499.
- Bentel, M.J., Yu, Y., Xu, L., Li, Z., Wong, B.M., Men, Y. and Liu, J. 2019. Defluorination of Per- and Polyfluoroalkyl Substances (PFASs) with

Hydrated Electrons: Structural Dependence and Implications to PFAS Remediation and Management. *Environmental Science & Technology* 53(7), 3718-3728.

Buxton, G.V., Greenstock, C.L., Helman, W.P. and Ross, A.B. 1988. Critical Review of rate constants for reactions of hydrated electrons, hydrogen atoms and hydroxyl radicals ($\cdot\text{OH}/\cdot\text{O}^-$ in Aqueous Solution. *Journal of Physical and Chemical Reference Data* 17(2), 513-886.

Cui, J., Gao, P. and Deng, Y. 2020. Destruction of Per- and Polyfluoroalkyl Substances (PFAS) with Advanced Reduction Processes (ARPs): A Critical Review. *Environmental Science & Technology* 54(7), 3752-3766.

Ding, X., Song, X., Chen, X., Ding, D., Xu, C. and Chen, H. 2022. Degradation and mechanism of hexafluoropropylene oxide dimer acid by thermally activated persulfate in aqueous solutions. *Chemosphere* 286, 131720.

Dixit, F., Barbeau, B., Mostafavi, S.G. and Mohseni, M. 2020. Efficient removal of GenX (HFPO-DA) and other perfluorinated ether acids from drinking and recycled waters using anion exchange resins. *Journal of Hazardous Materials* 384, 121261.

ECHA 2015 Background document to the Opinion on the Annex XV dossier proposing restrictions on Perfluorooctanoic acid (PFOA), PFOA salts and PFOA-related substances.

Fischer, M. and Warneck, P. 1996. Photodecomposition and Photooxidation of Hydrogen Sulfite in Aqueous Solution. *The Journal of Physical Chemistry* 100(37), 15111-15117.

Frisch, M.J., Trucks, G.W., Schlegel, H.B., Scuseria, G.E., Robb, M.A., Cheeseman, J.R., Scalmani, G., Barone, V., Petersson, G.A., Nakatsuji, H., Li, X.,

Caricato, M., Marenich, A., Bloino, J., Janesko, B.G., Gomperts, R., Mennucci, B., Hratchian, H.P., Ortiz, J.V., Izmaylov, A.F., Sonnenberg, J.L., Williams-Young, D., Ding, F., Lipparini, F., Egidi, F., Goings, J., Peng, B., Petrone, A., Henderson, T., Ranasinghe, D., Zakrzewski, V.G., Gao, J., Rega, N., Zheng, G., Liang, W., Hada, M., Ehara, M., Toyota, K., Fukuda, R., Hasegawa, J., Ishida, M., Nakajima, T., Honda, Y., Kitao, O., Nakai, H., Vreven, T., Throssell, K., Montgomery, J.A., Jr., J.E.P., Ogliaro, F., Bearpark, M., Heyd, J.J., Brothers, E., Kudin, K.N., Staroverov, V.N., Keith, T., Kobayashi, R., Normand, J., Raghavachari, K., Rendell, A., Burant, J.C., Iyengar, S.S., Tomasi, J., Cossi, M., Millam, J.M., Klene, M., Adamo, C., Cammi, R., Ochterski, J.W., Martin, R.L., Morokuma, K., Farkas, O., Foresman, J.B., D. J. Fox, G. and Inc., W.C. 2016 Gaussian 09, Revision A.02.

Galloway, J.E., Moreno, A.V.P., Lindstrom, A.B., Strynar, M.J., Newton, S., May, A.A. and Weavers, L.K. 2020. Evidence of Air Dispersion: HFPO-DA and PFOA in Ohio and West Virginia Surface Water and Soil near a Fluoropolymer Production Facility. *Environmental Science & Technology* 54(12), 7175-7184.

Gebbink, W.A., van Asseldonk, L. and van Leeuwen, S.P.J. 2017. Presence of Emerging Per- and Polyfluoroalkyl Substances (PFASs) in River and Drinking Water near a Fluorochemical Production Plant in the Netherlands. *Environmental Science & Technology* 51(19), 11057-11065.

Giri, R.R., Ozaki, H., Okada, T., Taniguchi, S. and Takanami, R. 2012. Factors influencing UV photodecomposition of perfluorooctanoic acid in water. *Chemical Engineering Journal* 180, 197-203.

- Glüge, J., Scheringer, M., Cousins, I.T., DeWitt, J.C., Goldenman, G., Herzke, D., Lohmann, R., Ng, C.A., Trier, X. and Wang, Z. 2020. An overview of the uses of per- and polyfluoroalkyl substances (PFAS). *Environmental Science: Processes & Impacts* 22(12), 2345-2373.
- Gomis, M.I., Vestergren, R., Borg, D. and Cousins, I.T. 2018. Comparing the toxic potency in vivo of long-chain perfluoroalkyl acids and fluorinated alternatives. *Environment International* 113, 1-9.
- Gonzalez, M.G., Oliveros, E., Wörner, M. and Braun, A.M. 2004. Vacuum-ultraviolet photolysis of aqueous reaction systems. *Journal of Photochemistry and Photobiology C: Photochemistry Reviews* 5(3), 225-246.
- Gu, Y., Liu, T., Wang, H., Han, H. and Dong, W. 2017. Hydrated electron based decomposition of perfluorooctane sulfonate (PFOS) in the VUV/sulfite system. *Science of The Total Environment* 607-608, 541-548.
- Han, X., Zhu, F., Chen, L., Wu, H., Wang, T. and Chen, K. 2020. Mechanism analysis of toxicity of sodium sulfite to human hepatocytes L02. *Molecular and Cellular Biochemistry* 473(1), 25-37.
- Heydebreck, F., Tang, J., Xie, Z. and Ebinghaus, R. 2015. Alternative and Legacy Perfluoroalkyl Substances: Differences between European and Chinese River/Estuary Systems. *Environmental Science & Technology* 49(14), 8386-8395.
- Hopkins, Z.R., Sun, M., DeWitt, J.C. and Knappe, D.R.U. 2018. Recently Detected Drinking Water Contaminants: GenX and Other Per- and Polyfluoroalkyl Ether Acids. *Journal AWWA* 110(7), 13-28.
- Jin, L. and Zhang, P. 2015. Photochemical decomposition of perfluorooctane

- sulfonate (PFOS) in an anoxic alkaline solution by 185nm vacuum ultraviolet. *Chemical Engineering Journal* 280, 241-247.
- Kiattisaksiri, P., Khan, E., Punyapalakul, P. and Ratpukdi, T. 2016. Photodegradation of haloacetonitriles in water by vacuum ultraviolet irradiation: Mechanisms and intermediate formation. *Water Research* 98, 160-167.
- Kim, T.-K., Lee, D., Lee, C., Hwang, Y.S. and Zoh, K.-D. 2022. Degradation of tetramethylammonium hydroxide (TMAH) during UV-LED/H₂O₂ reaction: Degassing effect, radical contribution, and degradation mechanism. *Journal of Hazardous Materials* 440, 129781.
- Lindstrom, A.B., Strynar, M.J. and Libelo, E.L. 2011. Polyfluorinated Compounds: Past, Present, and Future. *Environmental Science & Technology* 45(19), 7954-7961.
- Lu, T. 2014. Multiwfn. Software manual. Version 3(6).
- Lu, T. and Chen, F. 2012. Multiwfn: A multifunctional wavefunction analyzer. *Journal of Computational Chemistry* 33(5), 580-592.
- NIST 2022 The Radiation Chemistry Data Center of the Notre Dame Radiation Laboratory (ndrlRCDC) Kinetics Database.
- Olvera-Vargas, H., Wang, Z., Xu, J. and Lefebvre, O. 2022. Synergistic degradation of GenX (hexafluoropropylene oxide dimer acid) by pairing graphene-coated Ni-foam and boron doped diamond electrodes. *Chemical Engineering Journal* 430, 132686.
- Pan, Y., Zhang, H., Cui, Q., Sheng, N., Yeung, L.W.Y., Sun, Y., Guo, Y. and Dai, J. 2018. Worldwide Distribution of Novel Perfluoroether Carboxylic and Sulfonic Acids in Surface Water. *Environmental Science & Technology*

52(14), 7621-7629.

- Pica, N.E., Funkhouser, J., Yin, Y., Zhang, Z., Ceres, D.M., Tong, T. and Blotevogel, J. 2019. Electrochemical Oxidation of Hexafluoropropylene Oxide Dimer Acid (GenX): Mechanistic Insights and Efficient Treatment Train with Nanofiltration. *Environmental Science & Technology* 53(21), 12602-12609.
- Qu, Y., Zhang, C.-J., Chen, P., Zhou, Q. and Zhang, W.-X. 2014. Effect of initial solution pH on photo-induced reductive decomposition of perfluorooctanoic acid. *Chemosphere* 107, 218-223.
- Ren, Z., Bergmann, U. and Leiviskä, T. 2021. Reductive degradation of perfluorooctanoic acid in complex water matrices by using the UV/sulfite process. *Water Research* 205, 117676.
- Scientific, T.F. 2016. Thermo Scientific Orion Fluoride Ion Selective Electrode. User manual.
- Song, Z., Tang, H., Wang, N. and Zhu, L. 2013. Reductive defluorination of perfluorooctanoic acid by hydrated electrons in a sulfite-mediated UV photochemical system. *Journal of Hazardous Materials* 262, 332-338.
- Sun, M., Arevalo, E., Strynar, M., Lindstrom, A., Richardson, M., Kearns, B., Pickett, A., Smith, C. and Knappe, D.R.U. 2016. Legacy and Emerging Perfluoroalkyl Substances Are Important Drinking Water Contaminants in the Cape Fear River Watershed of North Carolina. *Environmental Science & Technology Letters* 3(12), 415-419.
- Suresh Babu, D., Mol, J.M.C. and Buijnsters, J.G. 2022. Experimental insights into anodic oxidation of hexafluoropropylene oxide dimer acid (GenX) on boron-doped diamond anodes. *Chemosphere* 288, 132417.

- Tomasi, J., Bonaccorsi, R., Cammi, R. and del Valle, F.J.O. 1991. Theoretical chemistry in solution. Some results and perspectives of the continuum methods and in particular of the polarizable continuum model. *Journal of Molecular Structure: THEOCHEM* 234, 401-424.
- Trang, B., Li, Y., Xue, X.-S., Ateia, M., Houk, K.N. and Dichtel, W.R. 2022. Low-temperature mineralization of perfluorocarboxylic acids. *Science* 377(6608), 839-845.
- UNEP 2019 The new POPs under the Stockholm Convention.
- USEPA 1999 Health effects from exposure to high levels of sulfate in drinking water study.
- USEPA 2020 User's Guide for T.E.S.T. (version 5.1) (Toxicity Estimation Software Tool): A Program to Estimate Toxicity from Molecular Structure.
- USEPA 2021 Human Health Toxicity Values for Hexafluoropropylene Oxide (HFPO) Dimer Acid and Its Ammonium Salt (CASRN 13252-13-6 and CASRN 62037-80-3) Also Known as "GenX Chemicals".
- USEPA 2022a Methodology document for the ecological structure-activity relationship model (ECOSAR) class program.
- USEPA 2022b Operation manual for the ecological structure-activity relationship model (ECOSAR) class program.
- Vakili, M., Bao, Y., Gholami, F., Gholami, Z., Deng, S., Wang, W., Kumar Awasthi, A., Rafatullah, M., Cagnetta, G. and Yu, G. 2021. Removal of HFPO-DA (GenX) from aqueous solutions: A mini-review. *Chemical Engineering Journal* 424, 130266.
- Wang, W., Maimaiti, A., Shi, H., Wu, R., Wang, R., Li, Z., Qi, D., Yu, G. and Deng, S. 2019a. Adsorption behavior and mechanism of emerging perfluoro-2-

propoxypropanoic acid (GenX) on activated carbons and resins. *Chemical Engineering Journal* 364, 132-138.

Wang, Y., Chang, W., Wang, L., Zhang, Y., Zhang, Y., Wang, M., Wang, Y. and Li, P. 2019b. A review of sources, multimedia distribution and health risks of novel fluorinated alternatives. *Ecotoxicology and Environmental Safety* 182, 109402.

Wang, Y. and Zhang, P. 2014. Effects of pH on photochemical decomposition of perfluorooctanoic acid in different atmospheres by 185nm vacuum ultraviolet. *Journal of Environmental Sciences* 26(11), 2207-2214.

Wu, Z., Shang, C., Wang, D., Zheng, S., Wang, Y. and Fang, J. 2020. Rapid degradation of dichloroacetonitrile by hydrated electron (e_{aq}^-) produced in vacuum ultraviolet photolysis. *Chemosphere* 256, 126994.

Zoschke, K., Börnick, H. and Worch, E. 2014. Vacuum-UV radiation at 185 nm in water treatment – A review. *Water Research* 52, 131-145.

6. Supporting Information

Table S1. Analysis conditions of HPLC-MS/MS for the analysis of GenX.	55
Table S2. Analysis conditions of HPLC-MS/MS for the analysis of TFA and PFPrA.	56
Table S3. Analysis conditions of UPLC-QTOF/MS for the identification of TPs.	57
Table S4. GenX degradation kinetics data ($[\text{GenX}]_0 = 0.30 \mu\text{M}$, VUV intensity ₂₅₄ $I_{\text{nm}} = 0.65 \text{ mW/cm}^2$, continuous N_2 purging; $n \geq 2$).	59
Table S5. Identified TPs of GenX during VUV photolysis and VUV/sulfite processes.	60
Table S6. Toxicity classification based on the Globally Harmonized System of Classification and Labelling of Chemicals (GHS).	63
Fig. S1. The molar distribution of S(IV) species in a solution as a function of pH. The species distribution was calculated with Visual MINTEQ 3.1 software.	64
Fig. S2. The optimized geometric structure of GenX at 6-311+g(d,p) level.	65

Table S1. Analysis conditions of HPLC-MS/MS for the analysis of GenX.

Instrument		Parameter	Condition	
HPLC-MS/MS	HPLC	Column	Phenomenex, Gemini C18 (2 × 50 mm, 3 μm)	
		Column temperature	40 °C	
		Injection volume	10 μL	
		Flow rate	0.25 mL/min	
		Mobile phase	(A) Deionized water with 20 mM ammonium acetate (B) Methanol	
			Time (min)	%B
			0.00	5
			3.00	40
			5.00	80
			8.00	80
	8.15	5		
	10.00	5		
	MS/MS	Ionization mode	ESI negative	
		Curtain gas	20 psi	
		Collision gas	4 eV	
		IonSpray voltage	-4500 V	
		Source temperature	500	
		Ion source gas 1	50 psi	
		Ion source gas 2	50 psi	
		Precursor ion / Product ion (m/z)	328.788 / 168.600	

Table S2. Analysis conditions of HPLC-MS/MS for the analysis of TFA and PFPrA.

Instrument		Parameter	Condition
HPLC-MS/MS	HPLC	Column	Restek, Raptor Polar X (2.1 × 50 mm, 2.7 μm)
		Column temperature	40 °C
		Injection volume	10 μL
		Flow rate	0.5 mL/min
		Mobile phase	(A) Deionized water with 0.05% formic acid + 10 mM ammonium formate (B) 60:40 Acetonitrile:Methanol with 0.05% formic acid
		Time (min)	%B
		0.00	85
		8.00	85
	MS/MS	Ionization mode	ESI negative
		Curtain gas	20 psi
		Collision gas	4 eV
		IonSpray voltage	-4500 V
		Source temperature	500
		Ion source gas 1	50 psi
		Ion source gas 2	50 psi
		Precursor ion / Product ion (m/z)	113.010 / 69.000 (TFA) 162.983 / 118.700 (PFPrA)

Table S3. Analysis conditions of UPLC-QTOF/MS for the identification of TPs.

Instrument		Parameter	Condition			
UPLC-QTOF/MS	UPLC	Column	Waters, ACQUITY UPLC BEH C18 (2.1 × 100 mm, 1.7 μm)			
		Column temperature	40 °C			
		Sample temperature	10 °C			
		Injection volume	10 μL			
		Flow rate	0.3 mL/min			
		Mobile phase	(A) Deionized water with 2 mM ammonium acetate (B) Methanol with 2 mM ammonium acetate			
				Time (min)	Flow (mL/min)	%A
		0.0	0.3	100	0	-
		0.5	0.3	80	20	6
		3.0	0.3	55	45	6
		6.0	0.3	20	80	6
		7.0	0.3	5	95	6
		8.0	0.3	5	95	6
		9.0	0.3	100	0	1
		10.0	0.3	100	0	1
QTOF/MS		Ionization mode	ESI negative			
		Acquisition range	50 – 1200 Da			
		Capillary voltage	1.5 kV			
		Cone voltage	40 V			

Collision voltage	Low: 4 V / High: 20 – 70 V
Desolvation temperature	250 °C
Source temperature	100 °C
Desolvation gas flow	800 L/h
Cone gas	0 L/h

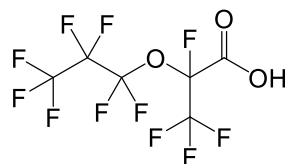
Table S4. GenX degradation kinetics data ($[\text{GenX}]_0 = 0.30 \mu\text{M}$, VUV intensity_{254 nm} = 0.65 mW/cm², continuous N₂ purging; n ≥ 2).

Treatment	Conditions	k_{obs} (min ⁻¹)	R ²
VUV photolysis	pH = 4	0.0038	0.993
VUV photolysis	pH = 6	0.0059	1.000
VUV photolysis	pH = 8	0.0034	0.986
VUV photolysis	pH = 10	0.0023	0.998
VUV/sulfite	[sulfite] ₀ = 4.80 mM; pH = 4	0.0011	0.909
VUV/sulfite	[sulfite] ₀ = 4.80 mM; pH = 6	0.0013	0.785
VUV/sulfite	[sulfite] ₀ = 4.80 mM; pH = 8	0.0033	0.953
VUV/sulfite	[sulfite] ₀ = 0.24 mM; pH = 10	0.0035	0.997
VUV/sulfite	[sulfite] ₀ = 0.80 mM; pH = 10	0.0068	0.990
VUV/sulfite	[sulfite] ₀ = 2.40 mM; pH = 10	0.0099	0.992
VUV/sulfite	[sulfite] ₀ = 4.80 mM; pH = 10	0.0113	0.988
VUV/sulfite	[sulfite] ₀ = 8.00 mM; pH = 10	0.0128	0.989
VUV/sulfite	[sulfite] ₀ = 12.0 mM; pH = 10	0.0150	0.980

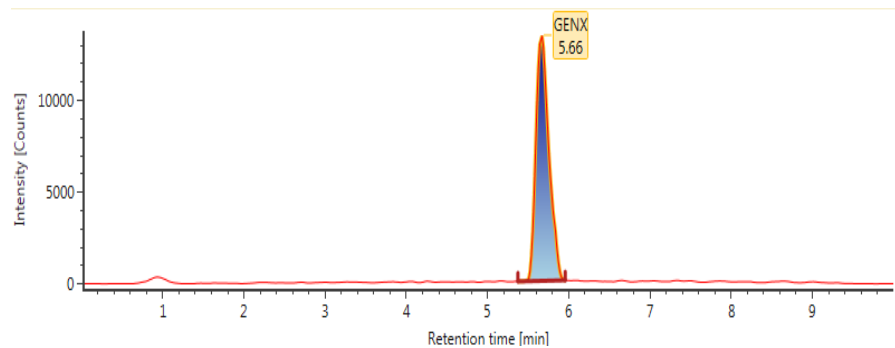
Table S5. Identified TPs of GenX during VUV photolysis and VUV/sulfite processes.

TPs	Formula	Observed RT (min)	Observed m/z	Adduct	Mass error (ppm)
GenX	C ₆ HF ₁₁ O ₃	5.66	329.9738	-H	-3.54

Structure

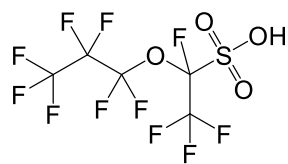


Chromatogram



TPs	Formula	Observed RT (min)	Observed m/z	Adduct	Mass error (ppm)
TP366	C ₅ HF ₁₁ O ₄ S	5.81	365.9426	-H	1.73

Structure



Chromatogram

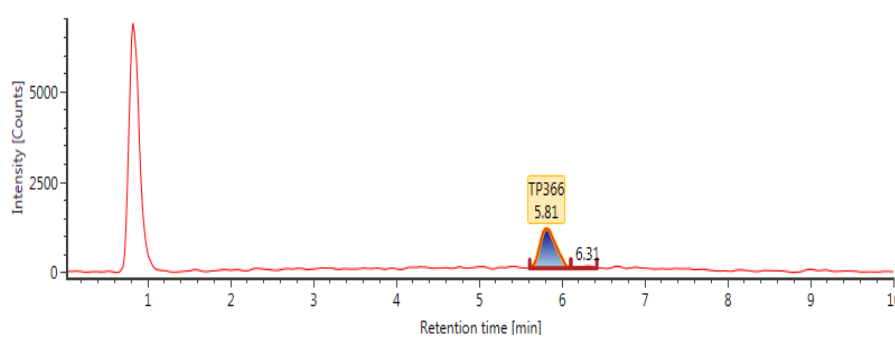
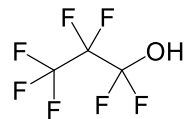


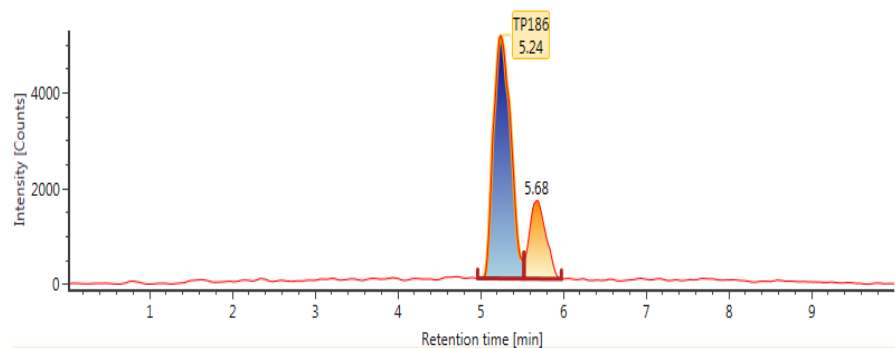
Table S5. (Continued)

TPs	Formula	Observed RT (min)	Observed m/z	Adduct	Mass error (ppm)
TP186	C ₃ HF ₇ O	5.24	185.9909	-H	-3.62

Structure

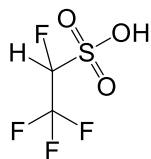


Chromatogram



TPs	Formula	Observed RT (min)	Observed m/z	Adduct	Mass error (ppm)
TP182	C ₂ H ₂ F ₄ O ₃ S	1.46	181.9650	-H	-5.71

Structure



Chromatogram

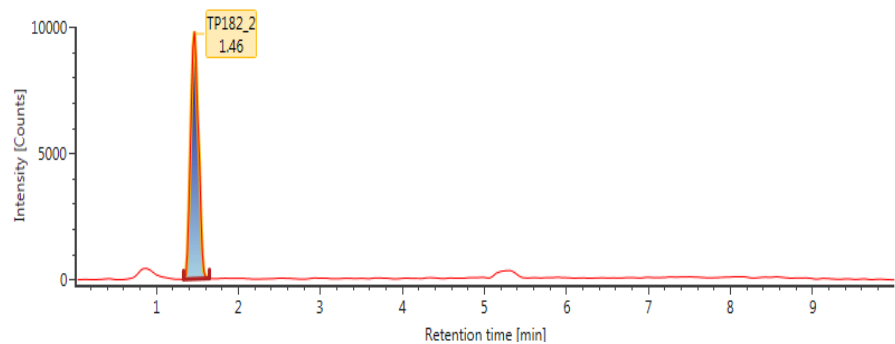
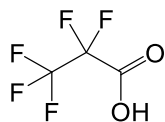


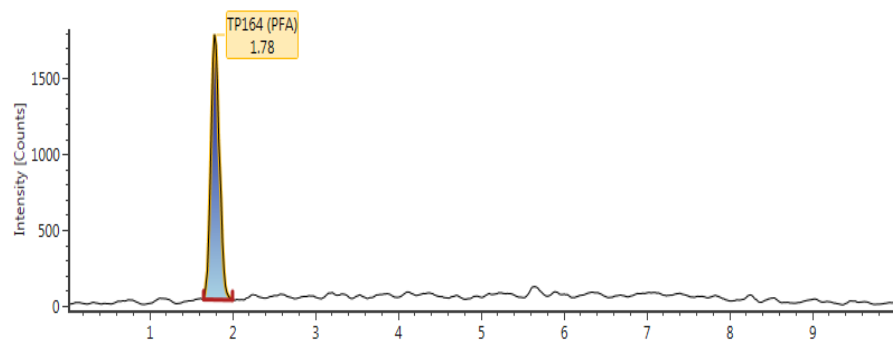
Table S5. (Continued)

TPs	Formula	Observed RT (min)	Observed m/z	Adduct	Mass error (ppm)
TP164	C ₃ HF ₅ O ₂	1.78	163.9888	-H	-5.32

Structure

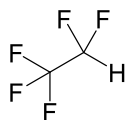


Chromatogram



TPs	Formula	Observed RT (min)	Observed m/z	Adduct	Mass error (ppm)
TP120	C ₂ HF ₅	1.78	119.9920	-H	-4.49

Structure



Chromatogram

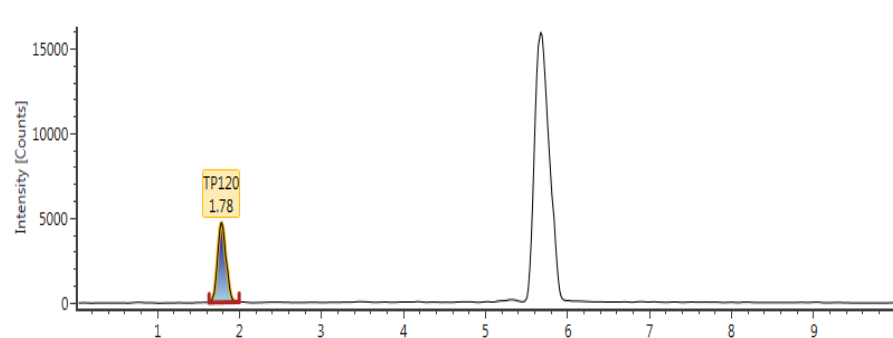


Table S6. Toxicity classification based on the Globally Harmonized System of Classification and Labelling of Chemicals (GHS).

Toxicity range (mg L ⁻¹)	Class	Toxicity range (mg kg ⁻¹)	Class
LC ₅₀ /EC ₅₀ /ChV ≤ 1	Very toxic	LD ₅₀ ≤ 5	Fatal if swallowed
		5 < LD ₅₀ ≤ 50	Fatal if swallowed
1 < LC ₅₀ /EC ₅₀ /ChV ≤ 10	Toxic	50 < LD ₅₀ ≤ 300	Toxic if swallowed
10 < LC ₅₀ /EC ₅₀ /ChV ≤ 100	Harmful	300 < LD ₅₀ ≤ 2000	Harmful if swallowed
100 < LC ₅₀ /EC ₅₀ /ChV	Not harmful	2000 < LD ₅₀ ≤ 5000	Maybe harmful if swallowed

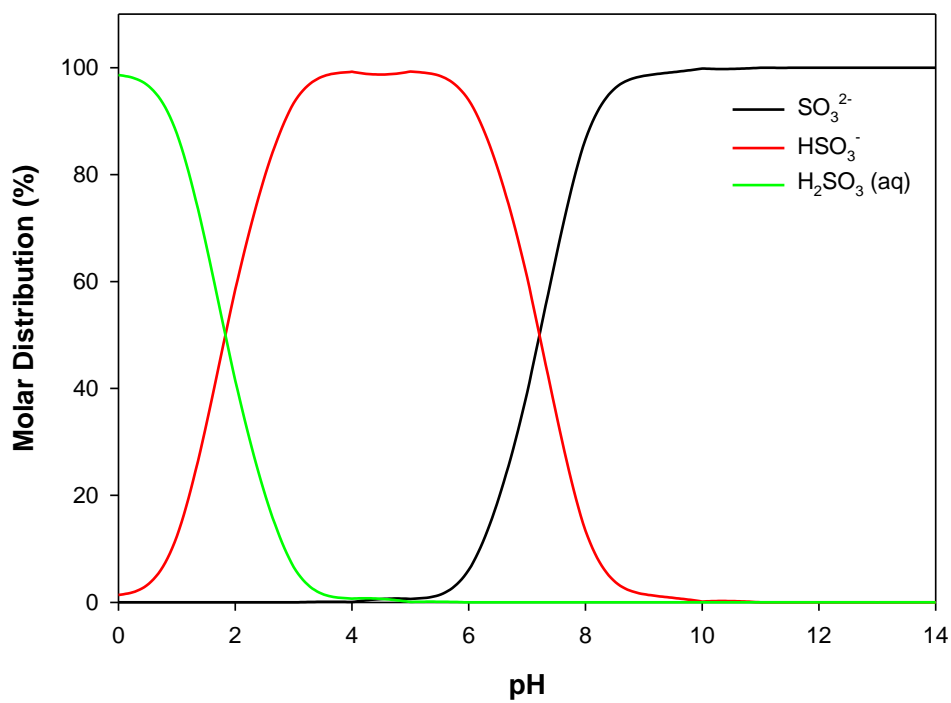


Fig. S1. The molar distribution of S(IV) species in a solution as a function of pH.

The species distribution was calculated with Visual MINTEQ 3.1 software.

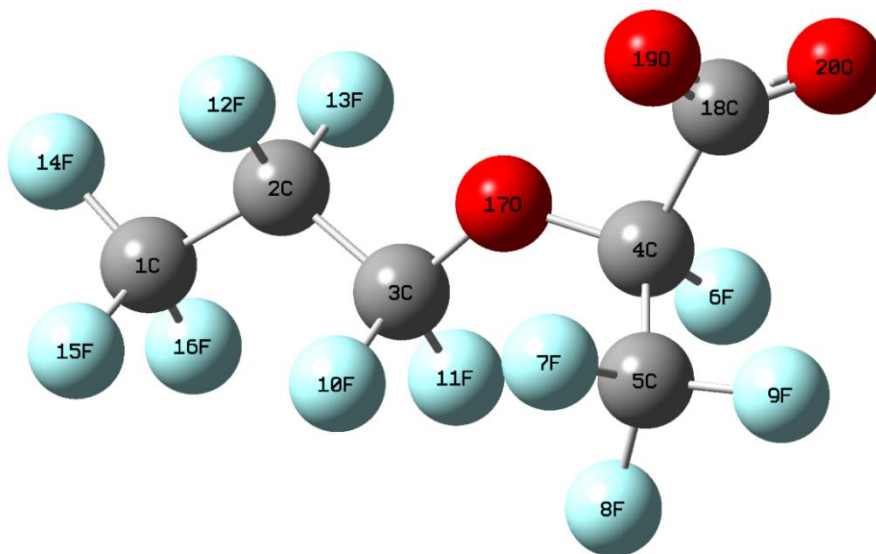


Fig. S2. The optimized geometric structure of GenX at 6-311+g(d,p) level.

국문초록

GenX라고 불리기도 하는 hexafluoropropylene oxide dimer acid(HFPO-DA)는 최근 다양한 수계에서 검출되고 있으며, 환경 내 잔류성과 독성으로 인해 우려의 대상이 되고 있다. 본 연구에서는 질소 포화 조건에서 진공자외선(VUV) 광분해와 VUV/아황산염(SO_3^{2-}) 반응 동안 수중 GenX의 분해를 연구하였다. 모든 반응에서 GenX의 분해 반응은 유사 1차 반응을 따랐다. VUV 광분해 반응에서는 pH 6에서 제거율이 가장 높게 나타난 반면, VUV/ SO_3^{2-} 반응에서는 높은 pH 조건에서 제거율이 증가하였다. 수산화 라디칼($\bullet\text{OH}$)은 GenX의 분해에 기여하지 않았으며, VUV/ SO_3^{2-} 공정에서는 부정적인 효과를 보였다. 두 반응에서의 GenX의 제거 부산물은 LC-MS/MS와 LC-QTOF/MS를 사용해 확인되었다. VUV 광분해 반응에서는 3개의 부산물(TFA, PFPrA, TP120)이 발견된 반면, VUV/ SO_3^{2-} 반응에서는 6개의 부산물(TFA, PFPrA (TP164), TP120, TP182, TP186, TP366)이 발견되었다. 또한 GenX의 탈불소화가 관찰되었으며, VUV 광분해와 VUV/ SO_3^{2-} 에서 각각 6시간 동안 17%와 67%의 탈불화율을 달성하였다. 식별된 제거 부산물과 친핵성 공격에 대한 반응성을 확인하는 이론적 계산을 기반으로 GenX의 분해 경로를 제안하였다. 분해 반응의 시작은 C-C 결합 절단, C-O 결합 절단 및 탈카르복실화 후의 설폰화로 확인되었다. 또한, ECOSAR 시뮬레이션을 이용한 생태 독성 예측은 분해 부산물의 독성을 간과해서는 안 된다는

것을 보여준다.

주요어 : GenX; 진공자외선; 수화전자; 수소 원자; 분해 부산물; 탈불소화